

Design and Fabrication of an Elastomer Based Variable Stiffness Device

Master Thesis

In partial fulfillment of the requirements for the degree

"Master of Science in Engineering"

Study program:

Mechatronics and Smart Technologies - Mechanical Engineering

Management Center Innsbruck

Supervisors:

Benjamin Massow, B.Sc., M.Sc.

Prof. David R. Clarke

Author:

David Altmann, B.Sc.

2110620016

Declaration in Lieu of Oath

„I hereby declare, under oath, that this master thesis has been my independent work and has not been aided with any prohibited means. I declare, to the best of my knowledge and belief, that all passages taken from published and unpublished sources or documents have been reproduced whether as original, slightly changed or in thought, have been mentioned as such at the corresponding places of the thesis, by citation, where the extend of the original quotes is indicated.“

Place, Date

Signature

Acknowledgement

First of all I, want to say thank you to my supervisors Benjamin Massow, B.Sc., M.Sc. from MCI | The Entrepreneurial School® and Prof. David R. Clarke from Harvard University for their commitment and support during my studies and my time abroad in the USA, giving me a chance many people can only dream of and broaden my knowledge in research, culture, and numerous other things.

I also want to say thank you to the members of Prof. Clarke's group, especially Gino Domel, David Farrell, and Miao Huo for helping and showing me countless things, as well as welcoming me in your group so warmly.

I want to thank my whole family, starting with my parents and sister Arabella, who support me since my first day with more than 100 % and have always been there for me, no matter what had to be solved. Thank you to my girlfriend, Isabella, for motivating me and having my back when going abroad and always being so encouraging.

Thank you to everyone helping finalizing my thesis and providing me with valuable feedback, especially Martin and Romed, for supporting me to find spelling and grammar mistakes.

Finally, I want to say thank you to everyone that I cannot say thank you anymore: my uncle Johannes, my grandmothers, my grandfather, and the best dog, Kaju. Everyone of you helped me so much!

Kurzfassung

Auf Elastomeren basierende Geräte mit variabler Steifigkeit sind eine neue Art von Aktuatoren, die durch ihre sekundenschnelle Zustandsänderung von hart auf weich und vice versa ein großes Potenzial für eine breite Palette von Anwendungen in der Soft-Robotik, Exoskeletten, Greifertechnologien und in verschiedenen medizinischen Geräten aufweisen. All diese Anwendungen können einen großen Einfluss auf Hilfsmittel haben, die Menschen unterstützen, welche entweder medizinische Hilfe oder Unterstützung bei der Arbeit benötigen (z.B. Baustellen, Prothesen, Gehhilfen oder Hebevorrichtungen). Die Implementierung solch eines Aktuators ermöglicht es ihren Nutzern, Tätigkeiten auszuführen, die zuvor schwer oder teilweise unmöglich waren. Ebenso ermöglicht es ihnen neue Aktuatoren zu verwenden, welche die Bewegungsgrenzen herkömmlicher Aktuatoren überschreiten und den Körper vor überanstrengenden Arbeitsbedingungen zu schützen. Bei der Entwicklung eines solch anspruchsvollen Geräts müssen in der Materialauswahl viele Aspekte berücksichtigt werden. Die Grundlage des Materialauswahlprozesses ist die Prüfung mit dem so genannten „Single Fiber Pull-Out Test“ und dem „Three-Point Beam Test“, die es ermöglichen, wertvolle Informationen über das Verhalten eines Elastomer-Faser-Verbunds zu sammeln. Diese Tests werden mit und ohne UV-Licht durchgeführt. Durch Einschalten des UV-Lichts verringert sich die Steifigkeit des Elastomers sekundenartig. Nach Ausschalten des UV-Lichts wird der Vorgang rückgängig gemacht und die Steifigkeit erhöht sich. Mit Hilfe der Analyse der Ergebnisse wird das am besten geeignete Material ausgewählt, um einen Prototyp zu entwerfen, der die grundlegenden Eigenschaften eines elastomerbasierten variablen Steifigkeit-Geräts zeigt. Es zeigt sich, dass durch sorgfältige Tests ein mit Glasfasern verstärktes, weiches Elastomer gefunden wurde, welches die Kriterien eines neuartigen Aktuators erfüllt. Hiermit ist ein erster, leicht herstellbarer Prototyp entwickelt worden, dessen Verbesserungen eingearbeitet und weiter untersucht werden sollen.

Schlagwörter: Soft-Robotik, CAN-Materialien, Medizintechnik, Elastomere, Materialauswahlverfahren

Abstract

Elastomer Based Variable Stiffness Devices are a new type of actuator with great potential for a wide range of applications in soft robotics, exoskeletons, gripper technologies and in various medical devices due to their extraordinary fast change of state from hard to soft and vice versa. All these applications can have a big impact in tools assisting and helping humans that either require medical support, or humans that need support while performing work (e.g. on construction sites, prostheses, walking assistance or lifting devices). The implementation of such an actuator enables their users to perform activities that were previously difficult or partially impossible. Likewise, it allows them to use new actuators that exceed the movement limits of conventional actuators and protect the body from overexerting working conditions. In order to develop such a sophisticated device, many aspects during the material selection phase have to be taken into account. The basis of the material selection process is the experimentation with the so-called “Single Fiber Pull-Out Test” and the “Three-Point Beam Test”, that allow to gather valuable information about the behavior of an elastomer and fiber composite. These tests have been done with and without the presence of UV-light, which allows the composite material to soften click-wisely when turned on, and to be stiff when turned off. By analyzing the obtained results, the most fitting material is chosen for the design of a prototype that shows the basic features. It turns out that through careful testing, a soft elastomer reinforced with glass fibers was found to meet the criteria of a novel actuator. An easy-to-make first prototype has been produced whose improvements will be incorporated and further investigated.

Keywords: Soft-Robotics, CAN-Materials, Medical-Technologies, Elastomers, Materials Selection

Contents

| | | |
|----------|--|----------|
| 1 | Introduction | 1 |
| 1.1 | Motivation | 1 |
| 1.2 | Task | 2 |
| 1.3 | Structure of the Thesis | 3 |
| 2 | Theoretical Background | 4 |
| 2.1 | Elastomers: Definition, Types, and Properties | 4 |
| 2.1.1 | Definition and General Types of Elastomers | 4 |
| 2.1.2 | Properties of Elastomers | 5 |
| 2.1.3 | Molecular Structure of Elastomers | 6 |
| 2.1.4 | Deformation and Stress-Strain Behavior of Elastomers | 7 |
| 2.1.5 | Applications of Elastomers | 8 |
| 2.2 | Elastic Modulus: Definition and Measurement | 8 |
| 2.2.1 | Definition and Theoretical Background of the E-Modulus | 8 |
| 2.2.2 | Variables Affecting the E-Modulus | 11 |
| 2.2.3 | Applications of Young’s Modulus and its Importance in Materials Science and Engineering | 11 |
| 2.3 | Covalent Adaptive Networks: Definition, Types, and Properties | 12 |
| 2.3.1 | Definition of Covalent Adaptive Networks | 12 |
| 2.3.2 | Types and Structure of Covalent Adaptive Networks | 12 |
| 2.3.3 | Effects of Covalent Adaptive Networks, and Their Applications | 13 |
| 2.4 | Properties of Composite Materials – Experimental Techniques and Their Basic Principles | 14 |
| 2.4.1 | Basics of the Single Fiber Pull-Out Test | 14 |
| 2.4.2 | Parameters Measured and Analyzed | 16 |
| 2.4.3 | Factors Affecting the Test Results | 17 |
| 2.4.4 | Applications of Single Fiber Pull-Out Tests | 18 |
| 2.4.5 | Three-Point Beam Test – Basics | 18 |
| 2.4.6 | Key Outputs of Three-Point Beam Test | 19 |
| 2.5 | Variable Stiffness Devices | 20 |
| 2.5.1 | Introduction to Variable Stiffness Devices | 20 |
| 2.5.2 | Types of Variable Stiffness Devices | 21 |
| 2.5.3 | Examples of Variable Stiffness Devices, and Their Applications | 22 |
| 2.5.4 | Definition of a Test-Schedule | 22 |

| | | |
|----------|--|-----------|
| 3 | Single Fiber Pull-Out Test | 23 |
| 3.1 | Materials Used for Testing | 23 |
| 3.1.1 | Selection Criteria and Characterization of Fiber and Matrix Materials | 23 |
| 3.1.2 | Mechanical and Physical Properties of Fiber and Matrix Materials | 23 |
| 3.2 | Experimental Setup | 24 |
| 3.2.1 | Design and Construction of the Testing Apparatus for a Single Fiber Pull-Out Test | 24 |
| 3.2.2 | Selection of Appropriate Test Parameters for Reliable and Reproducible Results | 26 |
| 3.2.3 | Detailed Procedure for Test Sample Preparation and Mounting in the Testing Apparatus | 27 |
| 3.3 | Data Analysis and Results | 29 |
| 3.3.1 | Analysis of Force-Displacement Diagrams | 30 |
| 3.3.2 | Overview of Experimental Data | 31 |
| 3.3.3 | Interpretation of Results | 34 |
| 3.3.4 | Preliminary Material Selection for the Variable Stiffness Device . | 36 |
| 4 | Three-Point Beam Test | 37 |
| 4.1 | Composite Materials Used for Testing | 37 |
| 4.1.1 | Options and Properties of Composite Materials | 37 |
| 4.1.2 | Manufacturing Procedure of the Composite Materials | 37 |
| 4.2 | Experimental Setup for the Three-Point Beam Test | 39 |
| 4.2.1 | Testing Apparatus for the Three-Point Beam Test | 39 |
| 4.2.2 | Test Parameters for the Three-Point Beam Test | 40 |
| 4.3 | Results and Data of the Three-Point Beam Test | 41 |
| 4.3.1 | Analysis of Force-Displacement Diagrams | 41 |
| 4.3.2 | Examination and Interpretation of the Collected Data | 43 |
| 4.3.3 | Final Material Selection for the Variable Stiffness Device-Prototype | 44 |
| 5 | Design and Manufacturing of a VSD-Prototype | 45 |
| 5.1 | Design Objective of the Prototype and Methodology | 45 |
| 5.1.1 | Design Concept and Requirements of the Prototype | 45 |
| 5.1.2 | Key Features and Functions | 45 |
| 5.1.3 | Technical drawings of the Variable Stiffness Device-Prototype . . | 46 |
| 5.2 | Actuation and Real Setup of the VSD-Prototype | 49 |
| 5.3 | Discussion of the Variable Stiffness Device-Prototype | 51 |
| 6 | Summary and Outlook | 53 |
| 6.1 | Summary | 53 |
| 6.2 | Outlook | 54 |
| | Bibliography | 59 |

| | |
|--|-------------|
| List of Figures | X |
| List of Tables | XI |
| List of Symbols | XII |
| Abbreviations | XIII |
| A Detailed Measurement Results – Single Fiber Pull-Out Test | XIV |
| A.1 Single Fiber Pull-Out Test – Glass Fiber | XV |
| A.2 Single Fiber Pull-Out Test – Steel Fiber | XVIII |
| A.3 Single Fiber Pull-Out Test – Nylon Fiber | XXI |
| B Source Code for Test Evaluation | XXIV |
| B.1 Source Code for Evaluation of Test Data | XXIV |
| B.2 Source Code for Creating a Heat-Map | XXVI |
| B.3 Source Code for Curve-Fitting | XXVII |

1. Introduction

1.1. Motivation

The production of precisely controllable Variable Stiffness Devices (VSDs) that can change their state reversible from hard to soft by activation of UV-light is important in various scientific fields such as soft-robotics and medical technologies. One of the most important goals is to provide adequate medical care for all people in hospital care and further treatments. While great progress is made in scientific research to meet this need, further development, detailed elaboration, and extensive testing are required to overcome the many challenges and difficulties in this field.

By actively addressing these challenges, a variety of benefits, such as improved automation capabilities, advances in miniaturization, and optimal reliability even under dynamic conditions is ensured. Pursuing these goals is critical to driving innovation and pushing the boundaries of what is possible.

A revolutionary class of VSDs emerges that is capable of significantly expanding the scope of applications and opening up breakthrough opportunities, particularly in the area of soft-robotics. A new material composition has been achieved through the combination of newly developed elastomers and so-called Covalent Adaptive Networks (CANs). This breakthrough enables rapid state changes within the actuator, providing precise control. In addition, these actuators exhibit fast and accurate responses, making them suitable for use in time-critical areas such as surgical procedures.

One of the main goals of this project is to find the ideal material composition in order to develop an endoscope, shown in Figure 1.1, that works as an elastomer based VSD. This innovative approach holds immense potential to revolutionize medical procedures by providing surgeons and medical doctors with a versatile tool that can dynamically adjust its stiffness.

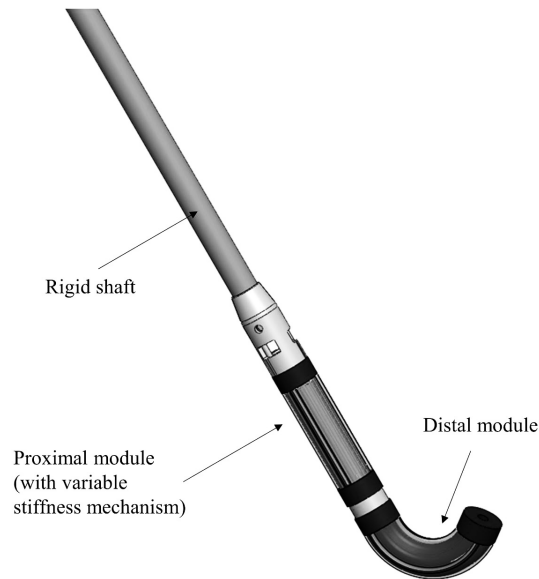


Figure 1.1.: VSD as an endoscope [1].

The ability to adjust the stiffness of an endoscope during examinations or procedures can greatly improve maneuverability and allow for more effective navigation through complicated anatomical structures while minimizing patient discomfort and preventing potential injuries.

The intended outcome of this thesis is to contribute to the advancement of VSDs by proposing a novel design and conducting comprehensive evaluations. By carefully investigating the performance, reliability, and practicality of the proposed endoscope, it hopes to provide a basis for the future development and implementation of VSDs in the medical field. In addition, the results will pave the way for further exploration of these VSDs in other critical applications, thus enabling innovation and progress in the field of soft-robotics and beyond.

The development of precision-controlled VSDs holds promise for a variety of applications. By focusing on the development of a VSD-Endoscope, this research is expected to help medical procedures and contribute to broader advances in soft-robotics and related fields. With this work, the aim is to access new possibilities of what can be achieved in the field of actuator technology.

1.2. Task

The main task is to design and fabricate an elastomer based VSD. This VSD ought to be able to conduct instantaneous changes of the stiffness in order to be versatile in different fields of applications. Before being able to design such a device, several tests and experiments must be executed, which is why the task can be split up into four different parts: the literature research with helping to get an overview over several

techniques and approaches, the Single Fiber Pull-Out Test where the preliminary material selection is done to go over into the next experiment, the Three-Point Beam Test that conducts a further, final material selection and specifies the material compositions that are used in the final part, the design of the VSD-prototype. The desired goal is a device, similar to an endoscope, that can be controlled by a UV-light source to change the stiffness and, ideally, to control the position of the actuator by wire-guidance. By doing all the necessary steps, the VSD needs to consist of an elastomer-fiber composite which shows a significant drop of the stiffness by activating the UV-light source. Moreover, the device should be a prototype that is able to be adapted and further developed by following research fellows and thesis projects and therefore consist of adaptable components.

1.3. Structure of the Thesis

Structurally, the present thesis is divided into four main chapters (Chapter 2 - Chapter 5), whereas Chapter 1 and Chapter 6 serve as an introduction, summary, and outlook and form the beginning and ending.

The theoretical background by means of the basics of elastomers, the definition and application of VSDs, insight to the elastic modulus (E-modulus), basics of covalent adaptive networks, the principles of the Single Fiber Pull-Out Test, and of the Three-Point Beam Test are discussed at the beginning (Chapter 2).

Following this, the preliminary material selection for the VSD-prototype is discussed. Part of this is the experimental setup with the various materials used, the test parameters, as well as the data analysis and results. This part of the thesis is crucial since the first step of the preliminary material selection for the VSD is made here (Chapter 3).

The final material selection process for the VSD-prototype, is fulfilled with the Three-Point Beam Test, containing the experimental setup, the different composite materials and the results. A detailed data analysis is covered in the final part. By completing the data analysis of both the Single Fiber Pull-Out Test and the Three-Point Beam Test, the final material selection is made (Chapter 4).

The manufacturing of the VSD-prototype is covered as the final part. Here, the design approach of the prototype, as well as the general idea is discussed. Moreover, the real actuation is investigated and a discussion on the actuation and its abilities is held. By this, the pro's and con's of the prototype are shown and improvement suggestions are made in the discussion on the VSD-prototype (Chapter 5).

2. Theoretical Background

2.1. Elastomers: Definition, Types, and Properties

2.1.1. Definition and General Types of Elastomers

As shown in Figure 2.1, elastomers are one of the six different materials subgroups in material engineering. Elastomers belong to the class of polymers, which tend to have a low E-modulus, show viscoelastic behavior and a very high strain before rupture [2].

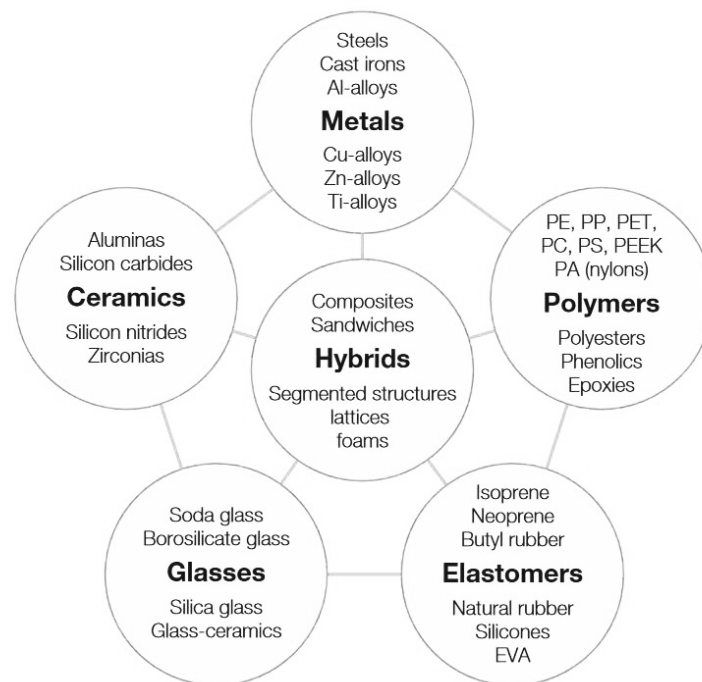


Figure 2.1.: Six families of materials science [3].

They can be used in many different fields of applications all over and have promising characteristics in new fields of engineering. Besides that, these kind of materials additionally show very high flexibility, good mechanical strength behavior, as well as curing behavior [4]. Elastomers are made of loose hydrocarbon chain polymers, which lead to the aforementioned elastic behavior above the so called glass-transition temperature T_g [5]. The glass-transition temperature characterizes the point where a solid or hard elastomer changes to a liquid or soft state. Elastomers may either be seen as an in-

dependent family, as shown in Figure 2.1, and in [3]. Other literature sources include them to the family of polymers as in [6] and [7].

As there exist various types of elastomers with different characteristics and structures, they can be divided into six classes [7]:

- **R class:** This kind of elastomer class consist of “backbones” completely made of carbon atoms with either single or double bonds. The double bonds hereby allow cross links with sulfur atoms but become very sensitive with oxygen and ozone atoms.
- **M class:** This subgroup of elastomers does not contain any carbon atoms or double bonds in their backbones. Because of this, the resistance against aging can be significantly improved.
- **O class:** As derived of their name, O class elastomers consist of oxygen atoms that are added to the carbon atoms in the backbone.
- **T class:** This class of elastomer contains sulfur atoms that are added to the carbon atoms inside the backbone.
- **U class:** In addition to the carbon atoms in the backbone, U class elastomers also consist of nitrogen and oxygen atoms.
- **Q class:** The final class of the elastomers, the so called Q class, has main chains made of oxygen and silicon atoms.

All these different classes of elastomers show specific properties. The different properties lead to different behavior under respective loads, such as tension, pressure, temperature differences, torsion and other kinds of load cases. Each load case requires different properties of the elastomer.

2.1.2. Properties of Elastomers

Like any other material, elastomers show various properties, which behave significantly different from conventional materials such as metals or related components. By dividing the properties into main classes, all different cases can be considered, depending on the use of the material. As elastomers belong to the family of polymers, elastomers show, compared to other materials like metals, very low E-moduli in the range of 10^{-3} GPa [3]. These are approximately 10^5 times smaller than the average metal [3]. Due to this, elastomers show very large deflections compared to the other material families and show a high strain before failure [3]. Occasional cross-links are the reason that allow elastomers to have such big displacements and are therefore called almost-linear polymer [6]. These cross-links' secondary bonds already melt at room temperature and cause the remembrance to the material to go back to its original shape after the load is removed [6]. In addition to the mechanical properties of elastomers, the electrical properties need to be considered as well. Due to the molecular structure, the

electrical conductivity of standard elastomers is very close to zero. Nevertheless, there are elastomers that can conduct electricity through the addition of additives like zinc oxide (ZnO) [8]. This gives elastomers an even wider range of applications by the addition and mixture of a wide variety of additive materials, which can adapt the molecular structure according to the desired properties. The thermal properties of elastomers can have a great influence on the mechanical behavior. In the process, the mechanical properties can change from brittle-elastic at low temperatures, viscoelastic and viscous behavior at high temperatures [6]. It is important to note that the melting point of elastomers is not only at very high temperatures, as in the case of metals or ceramics, but considerable changes in state also occur at room temperature [6]. That is why the glass-transition temperature T_g is of very high relevance in the field of research of elastomers [6].

2.1.3. Molecular Structure of Elastomers

Figure 2.2 shows the basic molecular structure of elastomers.

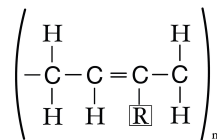


Figure 2.2.: Molecular structure of an elastomer [6].

The marked chemical element “R” indicates a placeholder, where different modifications of generic elastomers can be implemented. Adding chemical elements like Hydrogen H , Methanide CH_3 , or Chlorine Cl , different mechanical, thermal, electrical, and other properties can be manufactured [6]. Figure 2.3 illustrates the cross-linked bonds of elastomers under normal and loading condition.

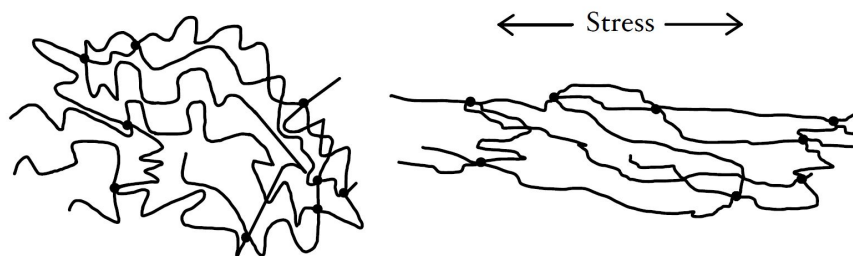


Figure 2.3.: Cross-linked elastomers in original (left) and deformed state (right) [5].

The weak, widely cross-linked amorphous bonds shown in Figure 2.3 lead to the typical behavior of elastomers. Per monomer unit, approximately one cross-link appears in every hundred monomer units [6]. The knotted structures of elastomers and their connecting points that firmly stabilize the structure under stress are clearly visible. In

general, elastomers are chemically bonded, which means that they cannot be melted [7].

2.1.4. Deformation and Stress-Strain Behavior of Elastomers

In Figure 2.4, the stress-strain behavior of different polymers, including elastomers can be seen. The stress-strain behavior of elastomers is very different from that of conventional metals, ceramics or other materials.

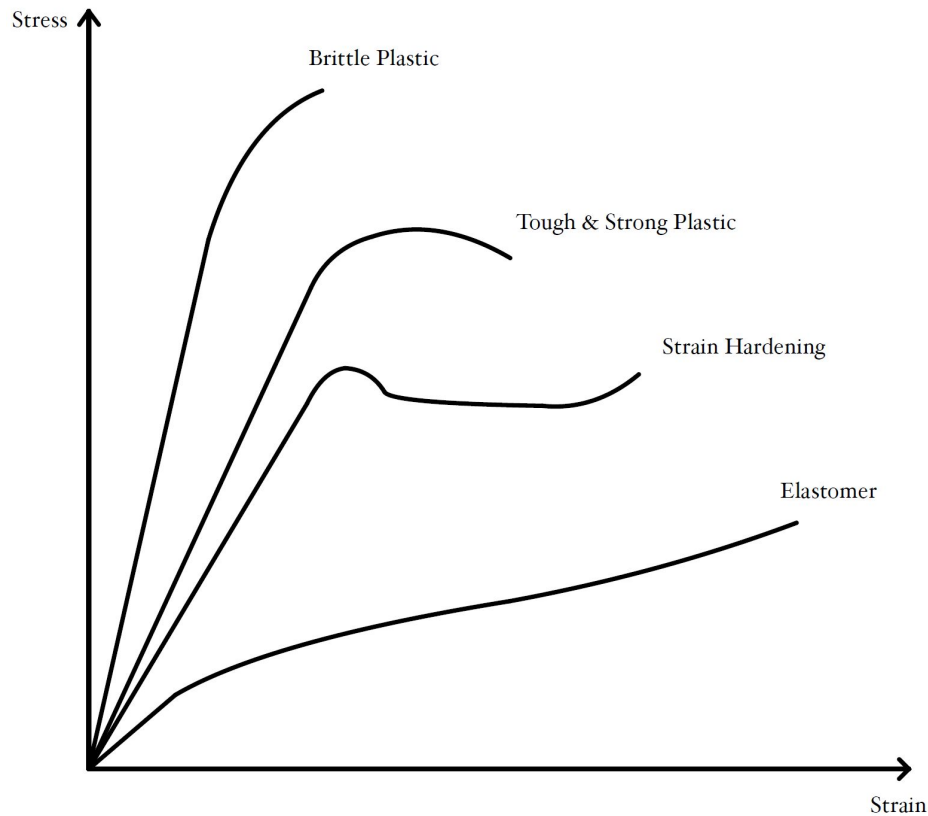


Figure 2.4.: Stress-strain curve of polymers [9].

The elastomers show an elastic behavior before rupturing. Compared to other polymer materials, elastomers have the lowest stress-strain curve. The reason for that is that elastomers typically have very low E-moduli and therefore have a very high elongation prior to rupturing [10]. Moreover, [10] describes that elastomers show a non-linear behavior of the stress-strain curve. What makes the behavior of elastomers so interesting is that elastomers can go back to its initial shape after having undergone a deformation of several times of their initial length. By having a look at Figure 2.3, the reason for that can be explained. The cross-links of the bonds clearly hold together the elastomer up until the point of rupture [10].

2.1.5. Applications of Elastomers

Due to the unique and essentially different properties of elastomers compared to other materials, elastomers are excellently suited for a wide range of applications shown in Figure 2.5.

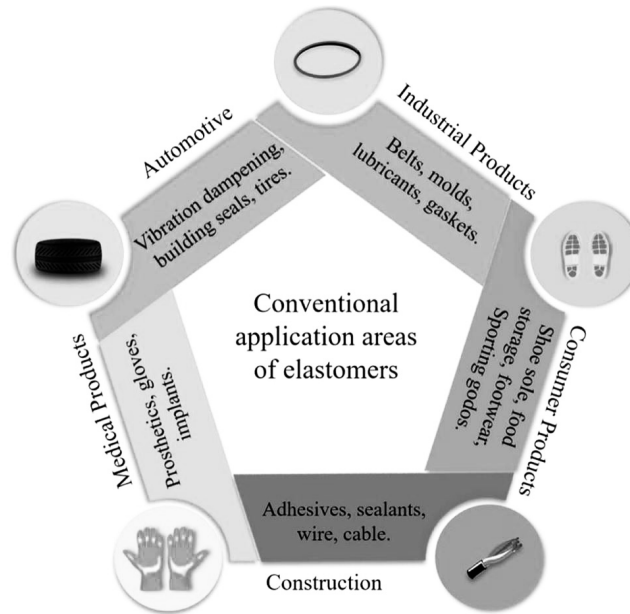


Figure 2.5.: Applications of elastomers [11].

The ability to absorb mechanical energy lets elastomers be the primary choice for tolerance components in bridges since vibrations can cause devastating outcomes [7]. Furthermore, elastomers find great usage in soft-robotics [12]. The soft properties that elastomers are attributed with, allow for various functional areas to be covered in such. An example of this would be an exoskeleton. A more illustrative application for elastomers would be in the automotive sector, e.g. in car tires. Beyond that: rubber bands, sealing rings, and elastomeric valves present further examples [12]. Besides the already mentioned applications, Figure 2.5 depicts more task areas, such as in the medical sector with prostheses or for consumer products with shoe soles and food storage [11].

2.2. Elastic Modulus: Definition and Measurement

2.2.1. Definition and Theoretical Background of the E-Modulus

In order to define the E-modulus, other properties have to be introduced first. A short pre-definition can be made for the E-modulus. According to [13], the E-modulus is a quantity that indicates the resistance of a material to elastic deformations. Giving an

example for a low E-modulus would be a material that deflects easily when a weight is attached to the middle of a beam which's endings rest on supports [13]. On the contrary, a high value of the E-modulus would be a material that hardly deflects by putting weights on it [13]. Introducing the first component of the E-modulus is done by defining the stress. The stress

$$\sigma = \frac{F}{A} \quad (2.1)$$

is defined as the force F acting on a component divided by A , the area of the component on which the force is acting.

An important note here is that the force F is acting normal to the surface. The stress σ is therefore called tensile stress with typical units of N mm^{-2} or MPa. The second essential parameter for the E-modulus is strain ϵ . It is defined by the response of a material when it experiences different stresses. Every material strains, some strain more (e.g. plastics), and some strain less (e.g. metals) [13]. The strain

$$\epsilon = \frac{u}{l} \quad (2.2)$$

can be defined as the ratio of u , the elongation or shortening of the sample, and l , the initial length of the sample. The strain can also be considered as

$$\epsilon(x) = \frac{du}{dx} \quad (2.3)$$

where the strain is defined as the derivative of the displacement at point x , as illustrated in Figure 2.6.

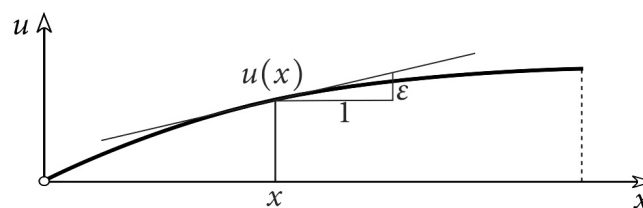


Figure 2.6.: Definition of strain by u-x diagram [14].

By having defined stress σ and strain ϵ , the definition of E-modulus can be made. The E-modulus is defined by the so-called “Hook’s Law”, which is only valid in the linear range of Figure 2.7. Hook’s law can be described by

$$\sigma = E\epsilon \quad (2.4)$$

and shows the relation between stress σ , strain ϵ and the E-modulus.

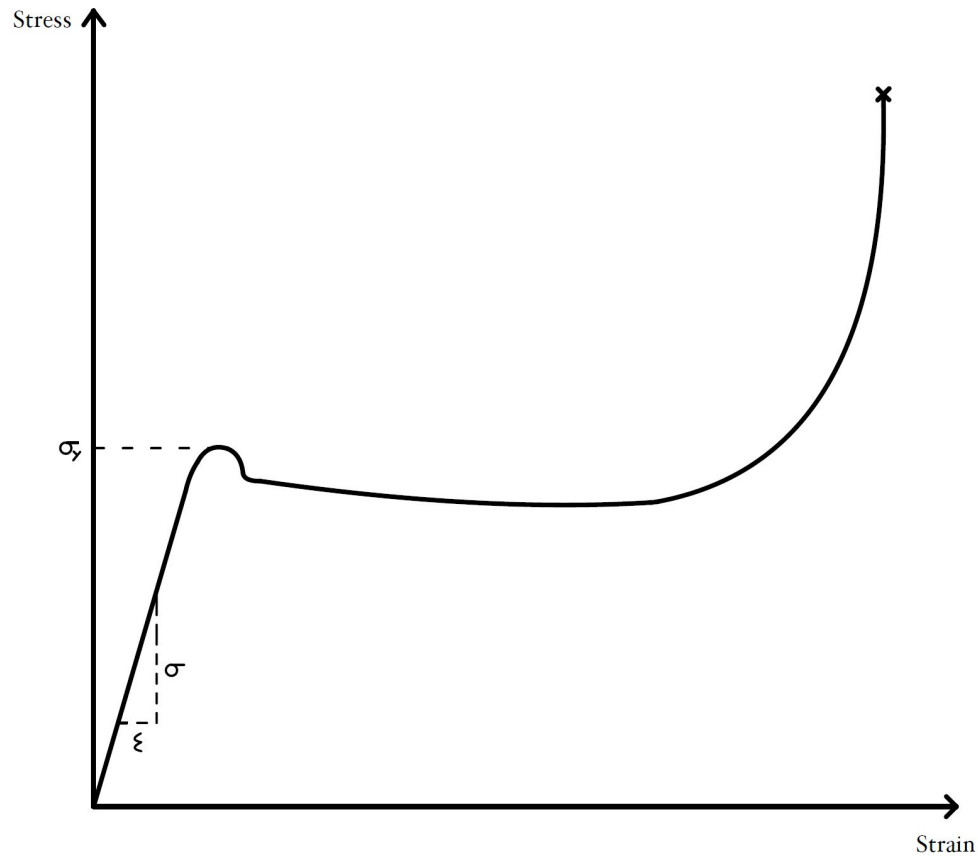


Figure 2.7.: Stress-strain curve of a polymer material [15].

Figure 2.7 shows the typical stress-strain curve of a ductile polymer. Since elastomers are part of the family of polymers, the figure above can be used to illustrate the corresponding behavior and explain the theory of Hook's law. As described before, Hook's law is only valid in the linear region of the stress-strain curve, which is at the very beginning of Figure 2.7. The slope in said figure describes the E-modulus of the material and is described by rearranging Equation 2.4 to

$$E = \frac{\sigma}{\epsilon} \quad (2.5)$$

where the E-modulus is defined by the ratio of the stress σ over the strain ϵ . By the end of the linear-elastic behavior, the yield stress σ_y is reached, which is defined as the beginning of the plastic behavior and the material yields. Until this level of stress is reached, the material can always go back to its original shape. Beyond that stress, the material has an irreversible plastic deformation and, by further elongation of the material due to the tensile test, the material will eventually fail due to rupture at the very end of the stress-strain curve [16].

2.2.2. Variables Affecting the E-Modulus

There are several variables affecting the E-modulus. By expanding the two parameters the influencing key figures become obvious, where

$$E = \frac{\sigma}{\epsilon} = \frac{\frac{F}{A}}{\frac{u}{l}} \quad (2.6)$$

can be further split into the ratio of force F and area A over displacement u and initial length l . The higher the force per area, and therefore the stress σ that the material can withstand in the elastic range, the higher the associated modulus will be. On the other side, the more strain the material experiences, the lower the E-modulus becomes. Another parameter that is influencing the E-modulus is derived from thermal strain

$$\epsilon_T = \alpha_T \Delta T \quad (2.7)$$

which basically depends on the coefficient of thermal expansion α_T and the temperature T . Therefore, the higher the coefficient of thermal expansion α_T , the higher the strain ϵ . Vice versa, the higher the temperature difference ΔT the higher the thermal strain ϵ_T . Equation 2.7 is only valid, if the temperature difference is uniform across the whole section, otherwise

$$\epsilon_T(x) = \alpha_T \Delta T(x) \quad (2.8)$$

is valid where ϵ_T and ΔT are dependent on the distance x [16].

2.2.3. Applications of Young's Modulus and its Importance in Materials Science and Engineering

In order to ensure adequate development of a component or product, the E-modulus is used to meet a wide variety of requirements. The requirements for engineering products with different E-moduli vary from bridges, car parts, medical technology devices, over to soft robotics, and sport devices. Therefore, all external influences, such as extreme temperature differences, different acting forces, various exposures and loads are taken into account during design processes; also defined in selection strategies [3]. The just mentioned external influences are called constraints [3]. The product has to withstand all of them in order to be eligible for production. The E-modulus plays a big role in a lot of these constraints, since the material should not be too heavy or light, should be either very stiff, or bendable e.g. a wing of a airplane or a variable stiffness device and should withstand extreme loads and a high number of load-cycles [3, 13]. Therefore, the E-modulus is a very powerful key figure to determine the strength, stiffness as well as the durability of a material. Besides these constraints, price will also

be a crucial factor during the design process and the decision for the material and its E-modulus. In summary, the E-modulus is part of every aspect of material selection, mechanical design, manufacturing engineering and is essential for understanding and predicting the behavior of materials and systems [3].

2.3. Covalent Adaptive Networks: Definition, Types, and Properties

2.3.1. Definition of Covalent Adaptive Networks

A rather unknown type of polymers and elastomers are CANs. These networks can adapt their molecular composition when a trigger is released [17]. By adjusting the composition in a way that suits best for the respective application; very useful applications can be developed. According to [17], CANs are networks that contain enough covalent bonds with a certain topology to allow the cross-linked network structure to chemically respond to an applied excitation. This chemical response is in general a certain change in either the stress, strain or state. The changes are achieved by a rearrangement of the network structure, where the initial bond density is retained [17]. Important here is that the process the material undergoes is typically reversible, therefore, no damage occurs to the material itself. As mentioned in [17] and [18], CAN materials belong to materials that are considered "smart", which get triggered by an external trigger and change their molecular composition and physical structure. Such external triggers can be for example temperatures, UV-light, mechanical forces and others [18].

2.3.2. Types and Structure of Covalent Adaptive Networks

Figure 2.8 shows an example for a molecular structure of a CAN that is also similar to the materials used in the project. In general, there are CANs that all have the same basic idea for their structure. These structures open new possibilities for polymers and elastomers with entirely new properties and applications. According to [18], the following CANs are the most common in this field:

- Photo-activated CANs
- Thermally activated CANs
- Mechanically activated CANs

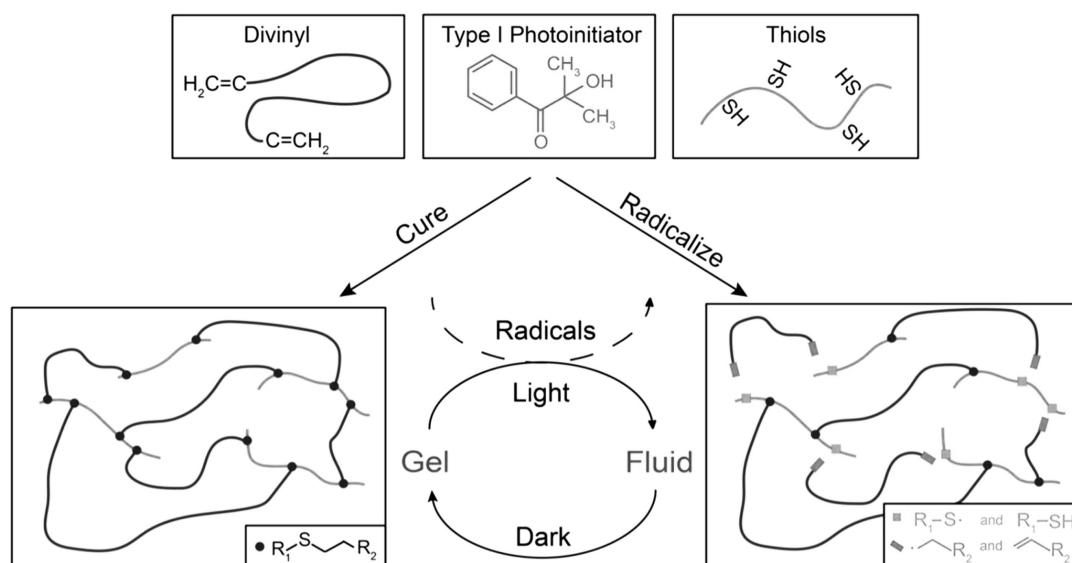


Figure 2.8.: Schematic structure of photo-activated CAN elastomers [19].

The material in Figure 2.8 is made up of Polydimethylsiloxane (*PDMS*) and the corresponding Divinyl and Thiol functional groups. Moreover, the material is made up of a Type 1 Photoinitiator, which is used to generate free radicals. The reaction taking place needs free radicals, since it is driven by radicals. The photo-initiator is needed for the activation of the trigger that finally acts as the stimulus of the CAN. After producing the sample by mixing together the 3 components, the mix has to be cured under UV-light in order to polymerize the sample. After curing, the CAN elastomer has the structure as in the bottom left part of Figure 2.8. Clearly visible are the cross-links and the bonding between Divinyl and Thiol after curing. Interestingly, when the material is triggered by the external stimulus (UV-light), a split-second change of the material from a gel like state to a fluid state happens [19]. By triggering the CAN, debonding of two groups occurs and the change of state is reached. This state change holds on, as long as the trigger is switched on. After switching the trigger off, the change to the solid state happens in a similarly fast way as from the solid to the fluid state [19]. Similar to the UV-light triggered CANs, other triggers such as reaching a given temperature or mechanical forces can be used [18].

2.3.3. Effects of Covalent Adaptive Networks, and Their Applications

As illustrated in Figure 2.9, an application for a CAN material can be a shape-morphing device. A typical effect of CANs is the fast stress relaxation for CANs with a low cross-link density [20]. An additional effect for CANs with a low cross-link density is that the flow activation energies are increasing due to that decreasing cross-link density.

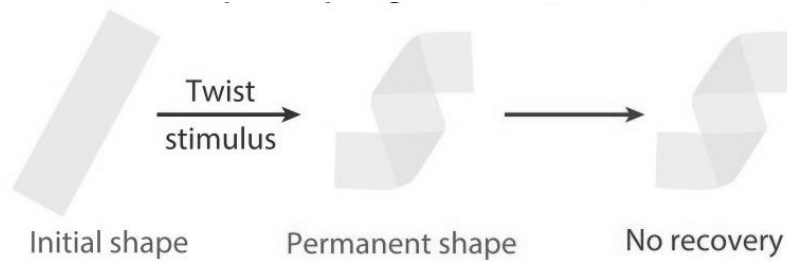


Figure 2.9.: Shape morphing device made of a CAN [21].

The material in Figure 2.9 has its initial shape and can be twisted to an arbitrary shape by applying the external stimulus. After switching off the stimulus, the material retains its shape until the external stimulus is turned on again.

CANs also find applications due to the following effects and possibilities, mentioned in [22]:

- Self-healing ability
- Recycling ability
- Reprocess ability

These points and effects cannot be achieved by conventional thermosets but by CANs [22]. Thermosets are a class of polymers where the cross-linking (curing) happens because of heat or another input, e.g. UV-light [23]. Besides that, thermosets have been through irreversible reactions at casting that makes it impossible to reform or recast them [23]. Due to the fact that those thermosets cannot meet the requirements for many applications, CANs take their place in those fields. These applications typically benefit from thermal, mechanical and further characteristics that thermosets usually do not have. This is the reason why CANs are used in devices that make them able to act as a reversible adhesive or to act as a crack-healing device [17]. Applications like these can be exercised in further expansion stages as well [17]. Some applications could be used for self-healing of two or more materials that were damaged e.g. due to too high mechanical forces [21]. By the self-healing ability, they are able to regain virgin-like properties [21]. More applications can be found in soft-robotics because of their abilities like easy deformation, elasticity and shape memory [24].

2.4. Properties of Composite Materials – Experimental Techniques and Their Basic Principles

2.4.1. Basics of the Single Fiber Pull-Out Test

A major component of this project is the Single Fiber Pull-Out Test with the basic structure illustrated in Figure 2.10.

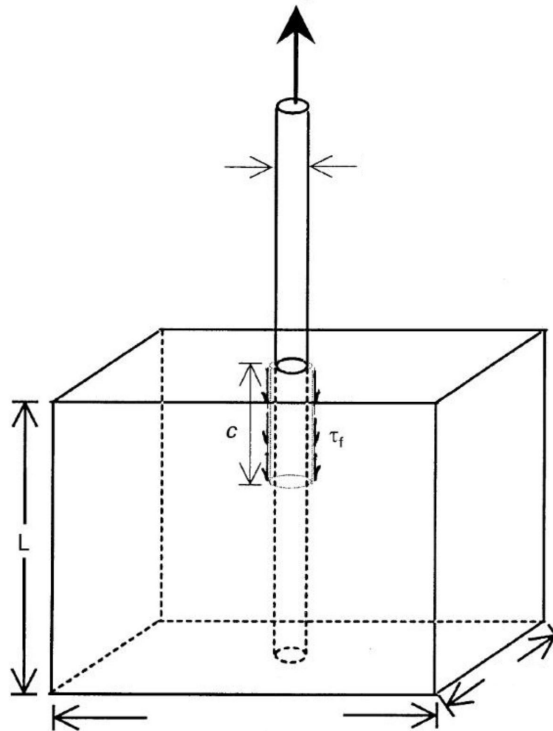


Figure 2.10.: Basic structure of the single fiber pull-out test [25].

The Single Fiber Pull-Out Test is, besides other test methods like the fragmentation test or micro-bond test, one method to investigate the bonding strength between an embedded fiber and a matrix [25]. This means that the interfacial properties, the interfacial shear strength and frictional stress can be described in more detail, as mentioned in [26]. As can be seen in Figure 2.10, a round fiber with a given diameter is embedded in a cube-like matrix of a material. This diameter is not necessarily specified, any diameter can be used and must be taken into account in the data analysis afterwards. The materials used as the matrix in this project are all elastomers. Other parameters in Figure 2.10 are L , the embedded fiber length presented as the dotted lines, c , the debonding length and τ_f , the acting interfacial shear strength [26]. The arrow at the top of Figure 2.10 shows the direction of the force applied to pull the fiber out of the matrix. Typically, the fiber is held by two clamps and the matrix is fixed on the other side by an embedding. This embedding is a mold, where the matrix material is poured in and gets solidified with a respective method.

Noticeable to see is what happens inside the composite material. Figure 2.11 shows the different stages during a Single Fiber Pull-Out Test.

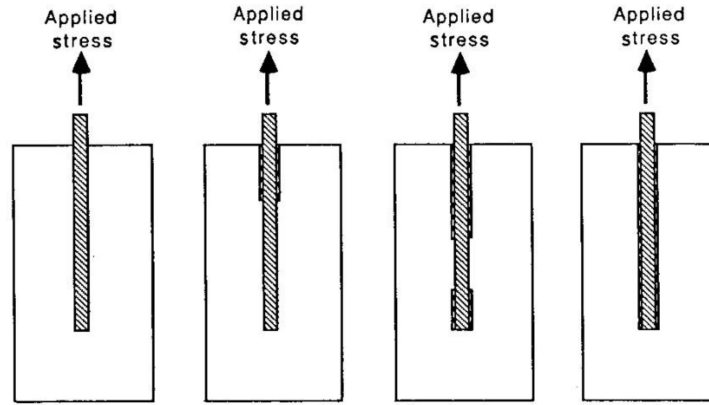


Figure 2.11.: Different stages during a single fiber pull-out test [27].

At the very beginning in Figure 2.11 (left), elastic behavior between the embedded fiber and matrix material is present [27]. By reaching the maximum force F_{max} , debonding either at one fiber end (Figure 2.11 (middle left)) or at both ends (Figure 2.11 (middle right)) occurs until the complete debonding of both phases seen in Figure 2.11 (right) [27].

2.4.2. Parameters Measured and Analyzed

By using the test setup as described in Chapter 2.4.1 and performing the test experiment, a force-displacement diagram as in Figure 2.12 results.

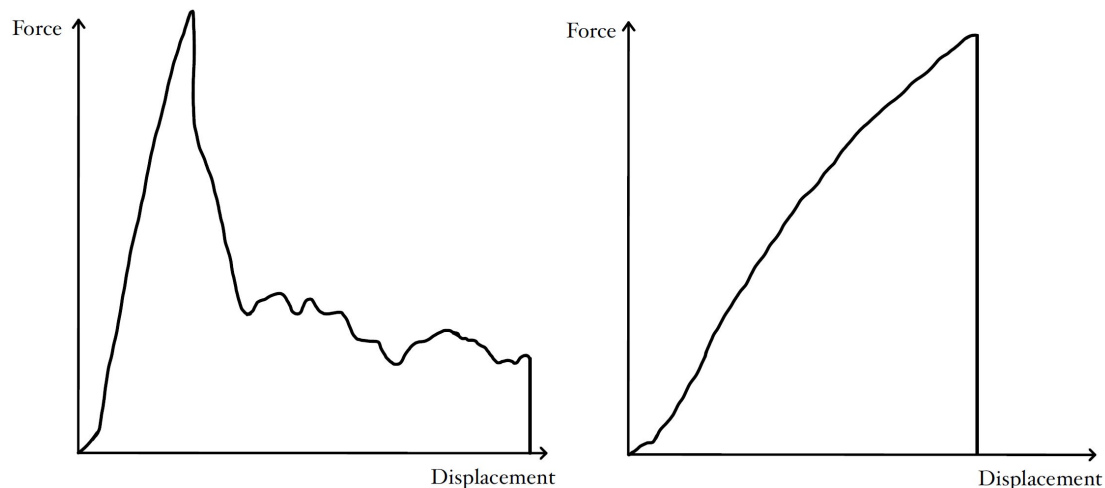


Figure 2.12.: Force-displacement diagram of a (left) valid & (right) invalid single fiber pull-out test [28].

The two plots in Figure 2.12 show a valid and an invalid test result for the Single Fiber Pull-Out Test. In order to correctly interpret the diagram, some parameters must be introduced first, which are:

- Maximum force F_{\max}
- Interfacial shear strength τ
- Fiber length l
- Fiber diameter d

F_{\max} can be seen easily in the force-displacement diagram and is the highest point, usually a peak, in it. After that peak, debonding between the embedded fiber and the matrix material occurs. Due to the debonding process, a drastic drop of the force can be seen in the diagram. Depending on the fiber and matrix material, rather steep or soft drops in the diagram occur and can therefore not be generalized. What can be said is that after the debonding, the diagram is dependent on the friction force between the fiber and the matrix, almost linear behaviors are not uncommon between fibers and elastomeric materials, which can be seen in subsequent chapters. The interfacial shear strength is given by

$$\tau = \frac{F_{\max}}{\pi \cdot d \cdot l} \quad (2.9)$$

the ratio of the maximum force F_{\max} over π , the diameter d , and the fiber length l is used [28]. By solving Equation 2.9, more knowledge about the strength and about the toughness of the composite material can be generated. Besides that, the tensile strength of a composite material becomes larger with τ [29].

In order to determine at which end the fiber is debonding first, [27] states a modified theory

$$\left(\frac{R^2}{r^2} - 1 \right) > \frac{E_f}{E_m} \quad (2.10)$$

where R is the radius of the matrix, r is the radius of the fiber and E_f and E_m are the corresponding E-moduli of the fiber and matrix material.

In case of Equation 2.10, the end where the load acts is debonding first [27]. If the left part is smaller than the right part of Equation 2.10, the embedded end is debonding first [27]. Further propagation information of debonding from the embedded end or from the loaded end can be found in [25].

2.4.3. Factors Affecting the Test Results

Various factors can influence the test results of the Single Fiber Pull-Out Test. The most important factors are:

- **Fiber Diameter and Geometry:** The diameter and shape of the fiber can affect the τ measured in a pull-out test. As can be seen in Equation 2.9, by having a

smaller fiber diameter or shorter fiber length, τ increases. Similarly, fibers with irregular or non-circular cross-sections may experience uneven stress distribution, leading to inconsistent test results [30].

- **Fiber/Matrix Adhesion:** The strength of the chemical and physical bond between the fiber and its matrix can affect τ in a single fiber pull out test. Stronger adhesion between the fiber and matrix will result in higher measured bond strengths [31].
- **Loading Rate:** The rate at which the load is applied during the Single Fiber Pull-Out Test can lead to a higher or lower F_{\max} and τ . A higher loading rate can have these effects due to the shorter time that is available for the bond to either fail or adapt to the conditions.
- **Environmental Conditions:** Another effect on the test results are the environmental conditions. As described in Chapter 2.1, factors such as temperature, humidity and also exposure to external effects like sun, etc. can impact results [32]. Therefore, it is of highest importance to assure the same conditions for every experiment.
- **Sample Preparation:** A crucial factor for the Single Fiber Pull-Out Test is consistent sample preparation, especially the alignment of the fibers. By annealing the fibers to be perfectly straight, as well as embedding them completely straight into the elastomer matrix, consistency for testing is assured. Furthermore, air bubbles inside the matrix material should be removed either by letting the air bubbles diffuse out of the sample over time or by putting the samples into a vacuum before curing. Also, the curing time under UV-light should be the same with every sample and the removing of specific mold parts must be done carefully.

2.4.4. Applications of Single Fiber Pull-Out Tests

Single Fiber Pull-Out Tests find various applications in the field of material science and especially in the examination of fiber and elastomeric matrices [33]. Instead of elastomeric matrices, every other matrix component can also be used, e.g. cement matrices [34]. By finding out more about the composite materials and the corresponding material behavior, decisions for which material to choose in a component can be made more easily. Furthermore, these tests can be carried out without great expense and without special technologies.

2.4.5. Three-Point Beam Test – Basics

A different experiment to determine the material's properties mentioned in Chapter 2.4 is the so called "Three-Point Beam Test". The basic experimental setup for this test procedure is illustrated in Figure 2.13.

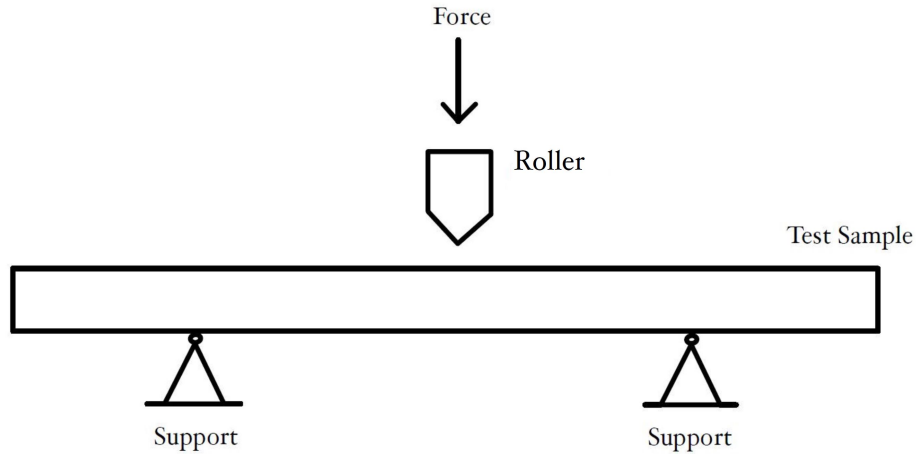


Figure 2.13.: Schematics of a basic three-point beam test.

The Three-Point Beam Test is consisting of three basic components: on the very top the roller is acting in a linear movement a force on the test sample, which is the second and most important component of the experiment. There exist many different forms of rollers for different compositions and applications. These rollers can either have a sharp or a round head and need to be properly chosen for the respective test procedure. The main advantage of the Three-Point Beam Test is the easy setup and preparation of the experiment [35]. Disadvantages are the high sensitivity of the results to the specimen, geometry and the strain rate. Moreover, the flexural properties are the final result of the Three-Point Beam Test since it is an effect of all three fundamental stresses: the tensile, compressive and shear stress [35].

2.4.6. Key Outputs of Three-Point Beam Test

A characteristic Force-Displacement diagram of a Three-Point Beam Test is shown in Figure 2.14. The stiffness can be calculated by

$$k = \frac{F}{x} \quad (2.11)$$

where F is the measured force and x the displacement.

The corresponding values are measured by the force sensor of the respective experimental unit and are plotted in a Force-Displacement diagram.

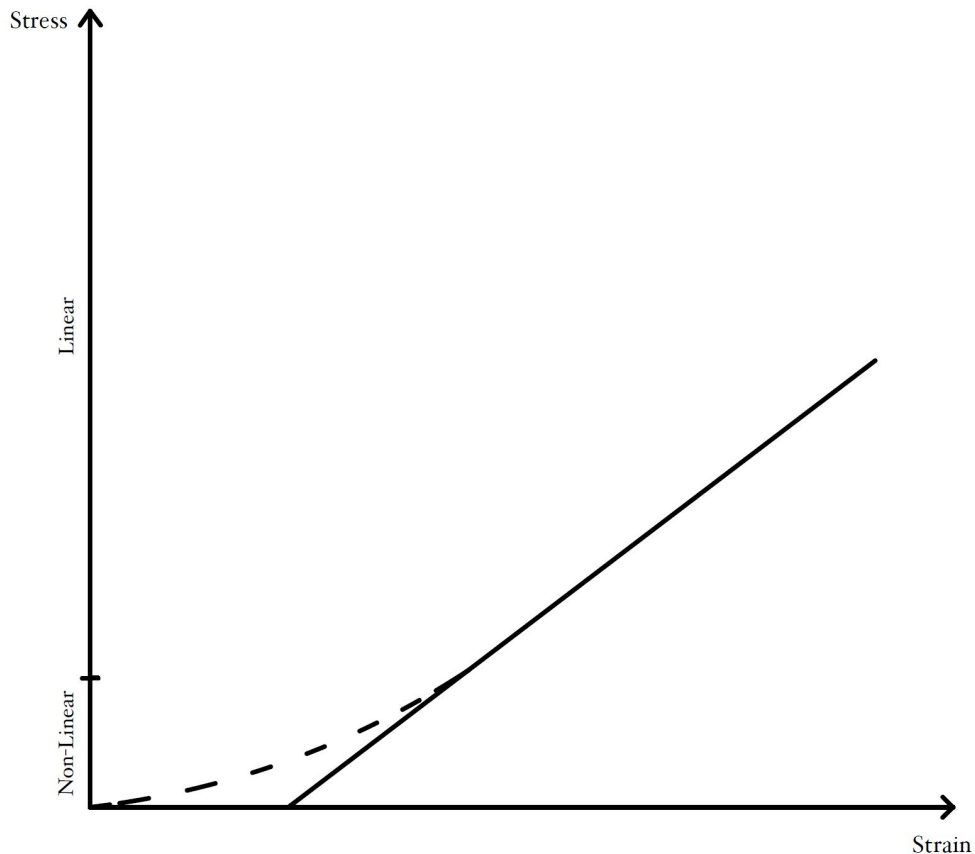


Figure 2.14.: Basic force-displacement curve of a three-point beam test [36].

The dashed line shows a non-linear behavior at the very beginning of the diagram. This region is non-linear because of the change of the contact area between the test sample and the roller [37]. Moreover, reaching the linear region in the diagram shows the deformation of the test sample in the direction of the thickness and the testing apparatus. The linear region is also the region of interest for obtaining the stiffness of the test sample. By curve fitting of the curve, k can be obtained easily with Equation 2.11.

2.5. Variable Stiffness Devices

2.5.1. Introduction to Variable Stiffness Devices

An example for a VSD is shown in Figure 2.15. The VSD is electrically actuated and can vary its stiffness by applying an electrical voltage V . The voltage is needed to trigger the dielectric elastomer and to compress the film, resulting in a stiffer overall performance of the VSD [38]. It also can be seen that the difference of stiffness without V and with V is changing in Figure 2.15. For the external load P , it is more difficult to act for more displacement.

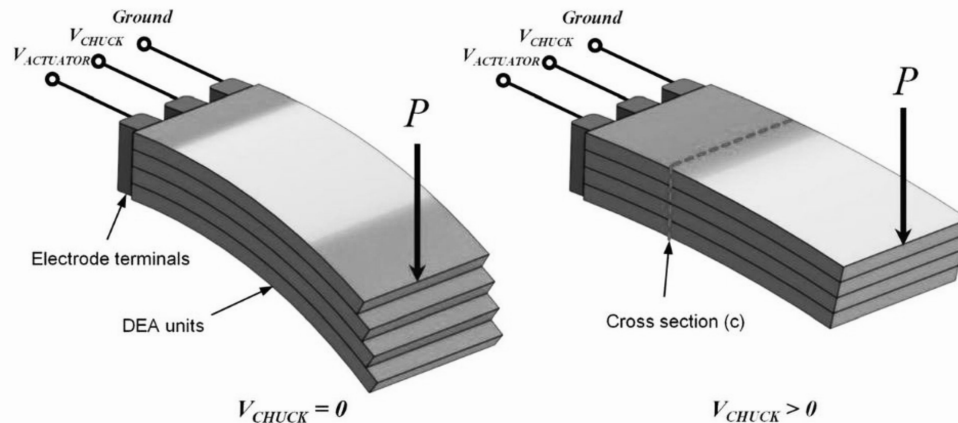


Figure 2.15.: Variable stiffness device with electrical actuation [38].

VSD's find a wide range of applications in robotics and are a subgroup of so called "Variable Impedance Actuators" [39]. It is also able that these robotic actuators do not include damping elements and they can be embedded in several robotic components [39]. Such robotic components may be found in fields like medicine, soft-robotics, vehicle engineering, aerospace applications and also wearable utilization [40]. What makes this type of actuator special is that the VSD is soft under a certain external stimulus and hard when the stimulus is removed.

2.5.2. Types of Variable Stiffness Devices

There are various types of VSD's with different triggers to achieve the change in stiffness to enable the desired actuation of the VSD. Listed below are the different types of VSD's and their working principles, as stated in [40].

- **Variable Rigidity Materials:** These kinds of materials experience a change in their molecular and microscopic structure. By doing that, the mechanical properties of the materials change as well and can hence be used for different applications. Examples for variable rigidity materials are shape memory alloys, thermo-plastic elastomers, and electro-mechanical conducting elastomers
- **Thermally Induced:** Another example for VSD's are thermally induced materials. As mentioned in Chapter 2.1, by reaching T_g or not, phase changes of the elastomer occur and also a change of the molecular structure. Again, the material's properties can change from a rigid state to a soft state and suitable applications can be found
- **Pressure Induced:** A simple type of VSD's are pressure induced VSD's. These types are common in granular materials, as well as in fluid-polymer composites. By inducing pressure p , click-like state changes of the material take place, which is feasible for applications in e.g. gripper technologies

- **Magnetic Field Induced:** This kind of VSD's is very widespread in magnetorheological fluids, elastomers and other networks that can be triggered magnetically. The materials here contain iron particles which change the viscosity of the material under the influence of the magnetic field. A use case for magnetic field induced VSD's, specifically magnetorheological elastomers, can be found in robotics and prosthesis
- **Others Types of Variable Stiffness Devices:** In addition to the just mentioned types of VSDs, there are other types which are mainly modifications of the ones listed. These modifications vary from different E-moduli to modified molecular structures.

2.5.3. Examples of Variable Stiffness Devices, and Their Applications

As discussed in the previous chapters, VSD's can be made of different materials and can therefore be activated by various stimuli. Common applications for VSD's can be found in soft-robotics and robotics [41, 42]. There, they can be used as soft-grippers to grab various objects with an undefined shape. The change can either be triggered pneumatically, electrically, or also by UV-light (CAN-networks). Additionally, VSD's are used in prosthetics and exoskeletons, where a typical application is a surgeon who needs to fix his arms at a certain height to achieve a satisfactory result at surgery [43]. Besides these applications, VSD's have a lot of potential for usage in the medical sector. Examples would be an endoscope or further designs and versions of prosthetics.

2.5.4. Definition of a Test-Schedule

Before being capable of designing a prototype of a VSD, Single Fiber Pull-Out Tests and the Three-Point Beam Tests have to be conducted. Doing this, the main characterizations like k , and F_{\max} of the composite materials can be figured out. To do this, a brief test-schedule has to be implemented. The first part and main part of the testings will be conducted by the Single Fiber Pull-Out Tests. These experiments are done with a variety of fibers, elastomers, and under varying UV-intensities. With that a broad spectrum of material compositions is intended to be covered and a shortlist of composite materials can be made with that. Once this shortlist has been compiled, the Three-Point Beam Tests are done. They mainly focus on the shortlist conducted before and the same compositions are tested but with different fiber densities and UV-intensities. After finally conducting the Three-Point Beam Tests, a final material choice for the VSD-prototype is made and further experiments can be fulfilled.

3. Single Fiber Pull-Out Test

3.1. Materials Used for Testing

3.1.1. Selection Criteria and Characterization of Fiber and Matrix Materials

Many elastomer and fiber materials have been considered before the final selection of such was made. Finally, the following materials listed in Table 3.1 are used.

Table 3.1.: Elastomer and Fiber Materials used in the Single Fiber Pull-Out Tests

| Elastomer Materials | Abbreviation | Fiber Materials |
|------------------------|-----------------|-----------------|
| V32/1V3T/SMS22/25SM21 | Low Material | Nylon |
| PDV/1V3T/SMS42/25SMS22 | Middle Material | Glass |
| V22/1V3T/SMS42 | High Material | Steel |

As can be seen in Table 3.1, the chemical composition of the materials get abbreviated as “Low”, “Middle”, and “High”. The reason for this is that the corresponding G-moduli are selected in a way that significant differences in magnitude between the elastomer materials are as great as possible in order to see the differences in behavior more obviously. A similar approach is used for the fibers: three materials with different bending-, and tensile-behavior are used to cover a large range of possible behaviors. Each fiber material is tested with each elastomer material. Furthermore, to gain more knowledge about the composite behaviors, all experiments are conducted with and without UV-illumination.

3.1.2. Mechanical and Physical Properties of Fiber and Matrix Materials

The characteristics of the elastomers are listed in Table 3.2. Particularly, two parameters are of main interest: the G-modulus and the Midpoint Switch Rate.

Table 3.2.: Characteristics of the Elastomers used in the Single Fiber Pull-Out Tests

| Material | G-modulus / kPa | Midpoint Switch Rate / % |
|-----------------|-----------------|--------------------------|
| Low Material | 5 | 58 |
| Middle Material | 60 | 15 |
| High Material | 125 | 12 |

As taken from Table 3.2, the differences of the G-moduli are big. The factor of magnification between the low- and middle-material is factor 12, between the middle- and high-material, the G-modulus is magnified by the factor 2.08. A decreasing trend can be seen at the Midpoint Switch Rate. Starting with a percentage of 58 % at the low material, the rate goes down to 15 % at the middle material and finally to 12 % at the high material. The characteristics of the three different fiber-materials can be taken from Table 3.3.

Table 3.3.: Characteristics of the Fibers used in the Single Fiber Pull-Out Test

| Material | Diameter/mm | Length/mm |
|----------|-------------|-----------|
| Nylon | 0.5 | 60.0 |
| Glass | 0.5 | 60.0 |
| Steel | 0.5 | 60.0 |

All the fibers have the same length of 60 mm and the same diameter of 0.5 mm, only the tensile and bending properties are different. This diameter is chosen because significantly smaller diameters show very low forces in the force-displacement curve and it is therefore more convenient to use the respective diameter. The length of the fibers can be chosen arbitrarily, it is important that the fiber is completely straight and does not bend when it is clamped in the setup.

3.2. Experimental Setup

3.2.1. Design and Construction of the Testing Apparatus for a Single Fiber Pull-Out Test

As a standardized test procedure for the Single Fiber Pull-Out Test does not exist, a few design options can be chosen freely during the design of the experimental setup. Figure 3.1 shows the test mold used in the Single Fiber Pull-Out Tests.

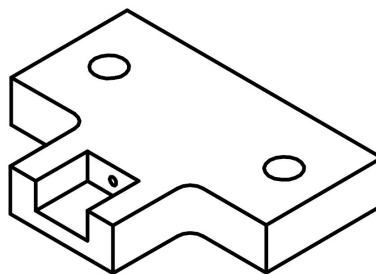


Figure 3.1.: Side-view of the test mold.

The most important criteria is to ensure a repeatability and consistency of all experiments and respectively the same conditions. For a complete testing apparatus, six

main components must be put together:

- Test Mold
- Elastomer
- Fiber
- Clamp-Mounting
- Force Sensor - Futek[®]-LSB200
- Horizontal Motion Sled

These components ensure the proper and reliable execution of the experiments. Nevertheless, the first three components are the most important since they have to be put together in the right order and meet certain requirements. Most important is that the test mold has one open side for the composite material and has to not be constrained by a wall or mounting. If the composite material were to be constrained by a wall, the results of the experiments would be erroneous and can therefore not be used for further evaluations.

Figure 3.2 and Figure 3.3 show the top-view and front-view of the test mold. The drillings with a diameter of 5.50 mm are used for mounting the test mold and the small drilling with a diameter of 1.35 mm is for alignment purposes of the fiber. The top-view perspective on the test mold shows the most important dimensions of the test mold.

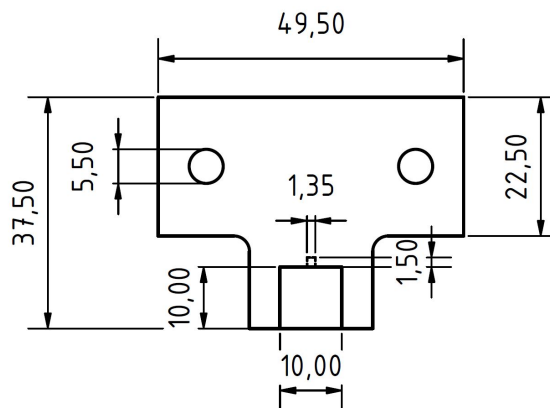


Figure 3.2.: Top-view of the test mold.

Another crucial requirement of the test mold is the quadratic shape where the composite material is inside. The overall shape of the component is related to the setup in the laboratory and the mounting fixed to the horizontal motion sled. Besides the quadratic shape of 10 mm \times 10 mm, the depth of the composite material is 5 mm.

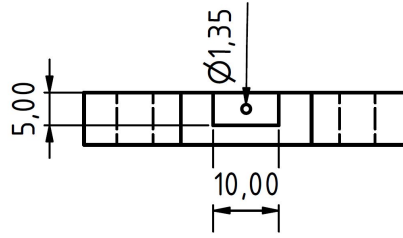


Figure 3.3.: Front-view of the test mold.

The test molds and clamp-mountings are produced by rapid-manufacturing with the Ender[®] 5 Plus 3D-printer. Each test mold can be reused after the experiment is done and afterwards just has to be cleaned. Following this, the procedure discussed in Chapter 3.2.3 must be applied. Besides the test mold, two further components are listed in the enumeration: the force-sensor and the horizontal motion sled. For the correct plotting of the data, the force-sensor Futek[®]-LSB200 in combination with a LabVIEW[®] program is responsible. The characteristics and specifications are listed in [44]. The horizontal, separating movement is conducted by the motion sled. It separates the clamp-mounting and the test mold with a constant speed and for a given distance.

3.2.2. Selection of Appropriate Test Parameters for Reliable and Reproducible Results

The test parameters of the Single Fiber Pull-Out Test are listed in Table 3.4. The consistency of the data is of utmost importance to be able to make a fundamental pre-material selection.

Table 3.4.: Test Parameters - Single Fiber Pull-Out Test

| Test Procedure | Acceleration / mm s^{-2} | Velocity / mm s^{-1} | Distance / mm | Intensity / % |
|----------------|-----------------------------------|-------------------------------|---------------|---------------|
| No UV | 100.0 | 0.1 | 11.0 | 0.0 |
| UV | 100.0 | 0.1 | ≥ 11.0 | 1.0 |
| UV | 100.0 | 0.1 | ≥ 11.0 | 5.0 |
| UV | 100.0 | 0.1 | ≥ 11.0 | 10.0 |

The acceleration is relatively high in order to be able to transition to a speed of 0.1 mm s^{-1} immediately. Furthermore, the velocity is kept at a very low speed to let the composite material adapt to the displacement and deformations. If the velocity has a higher value, the data cannot be used due to the noise and insufficient precision. To ensure the complete separation of the fiber and elastomer matrix, a distance of 11 mm is used for the experiments without UV-light. A bigger distance must be used for the experiments with UV-light, because the composite material changes its behavior drastically and can also get softer, which is why greater distances must be covered. The last parameter is the intensity of the OmniCure[®] S2000 with an intensity of 30 W cm^{-2} .

When conducting the experiments with UV-light, one test each with 1 %, 5 %, and 10 % of the maximum intensity is carried out.

3.2.3. Detailed Procedure for Test Sample Preparation and Mounting in the Testing Apparatus

First the test mold from Figure 3.4 must be printed out with the Ender[®] 5 Plus 3D-printer. The next step is to poke a hole with a needle into the Very High Bond-foil (VHB) that has to be pecked to the open side of the test mold to avoid the outflow of the liquid elastomer before the curing process. The corresponding fiber is put into this hole and has to be aligned perfectly straight. The steel and the glass fibers are already aligned. In order to achieve this for the nylon fiber, they have to be annealed in an oven at 125° C for at least twelve hours in a cast to straighten the fibers.



Figure 3.4.: Empty test mold.

After annealing the fibers, they are put into the hole of the VHB-foil and test mold. Next, the respective elastomer is poured into the mold. Having done this, the mold is put into a UV-chamber. There it is cured under UV-light for twelve minutes by the simultaneous addition of nitrogen which helps the material to preserve its photo-switchable characteristics. Figure 3.5 shows the test mold after the curing process. Here, the elastomer is in a solid, gel-like state and the fiber sticks to the elastomer. A composite material is formed.

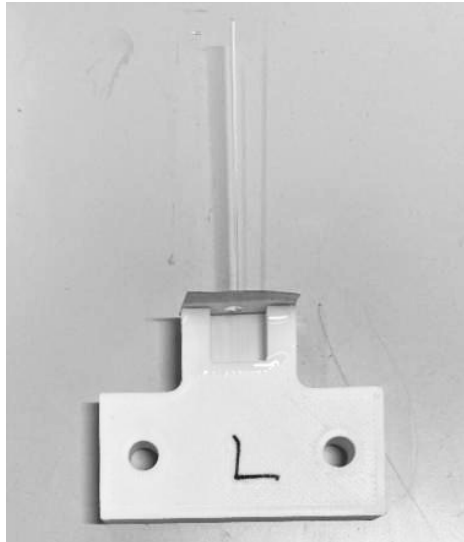


Figure 3.5.: Filled test mold.

Figure 3.6 shows the last step before the test mold can be completed. Here, the VHB-foil must be removed gently from the mold and elastomer. By completing this step, a test mold for the Single Fiber Pull-Out Test is produced.

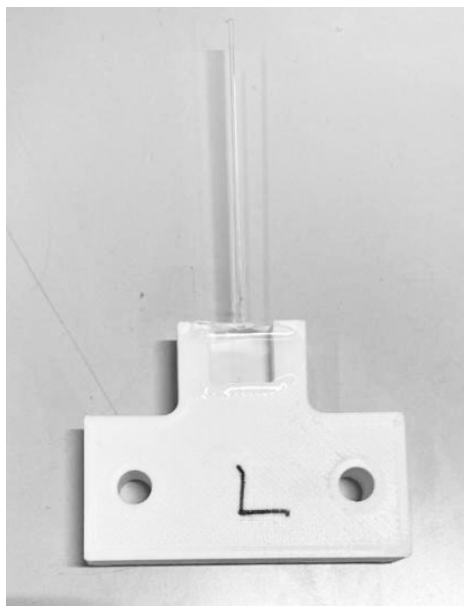


Figure 3.6.: Complete test mold.

Since the test mold is ready for the experiment, it can be put together in order to complete the experimental setup shown in Figure 3.7. In the right part of Figure 3.7, the test mold is fixed in the embedding. The left part shows the clamp-mounting where the fiber is fixed in between.

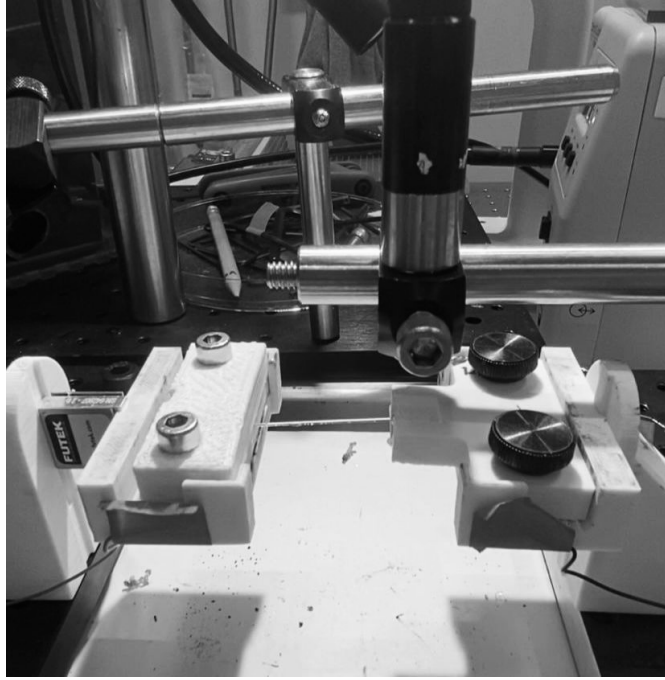


Figure 3.7.: Final experimental setup.

It can be necessary to use VHB-foil at the clamp-mounting to prevent the fiber from slipping. This is the general experimental setup for the Single Fiber Pull-Out Test without UV-light. In the case of UV-light illumination, the OmniCure[®] S2000 is used. The glass tube is coming from the top and shines the UV-light directly onto the composite material. By that, the chemical and mechanical composition is subject to a change which's results are discussed in Chapter 3.3. These results are plotted in a force-displacement graph. The forces are measured by the force-sensor in the left part of Figure 3.7, the displacement is output of the horizontal motion sled that is pulling the fiber out of the elastomer matrix and therefore separating the two faces.

3.3. Data Analysis and Results

By setting up the experimental setup and conducting all variations of Single Fiber Pull-Out Tests shown in Table 3.5, the analysis and evaluation of the experimental data is crucial for the preliminary material selection.

Table 3.5.: Experiment Composition of the Single Fiber Pull-Out Tests

| Elastomer Material | Fibers | UV-Intensity / % |
|--------------------|--------|------------------|
| Low Material | Nylon | 1 |
| Low Material | Glass | 1 |
| Low Material | Steel | 1 |
| Low Material | Nylon | 5 |
| Low Material | Glass | 5 |
| Low Material | Steel | 5 |
| Low Material | Nylon | 10 |
| Low Material | Glass | 10 |
| Low Material | Steel | 10 |
| Middle Material | Nylon | 1 |
| Middle Material | Glass | 1 |
| Middle Material | Steel | 1 |
| Middle Material | Nylon | 5 |
| Middle Material | Glass | 5 |
| Middle Material | Steel | 5 |
| Middle Material | Nylon | 10 |
| Middle Material | Glass | 10 |
| Middle Material | Steel | 10 |
| High Material | Nylon | 1 |
| High Material | Glass | 1 |
| High Material | Steel | 1 |
| High Material | Nylon | 5 |
| High Material | Glass | 5 |
| High Material | Steel | 5 |
| High Material | Nylon | 10 |
| High Material | Glass | 10 |
| High Material | Steel | 10 |

Per composite material, three experiments are conducted with, and three without UV-illumination (one per respective UV-intensity).

3.3.1. Analysis of Force-Displacement Diagrams

In order to evaluate the measured values correctly, the force-displacement diagrams are analyzed with a curve-fitting tool shown in Figure 3.8. The source code is attached in Appendix B.3.

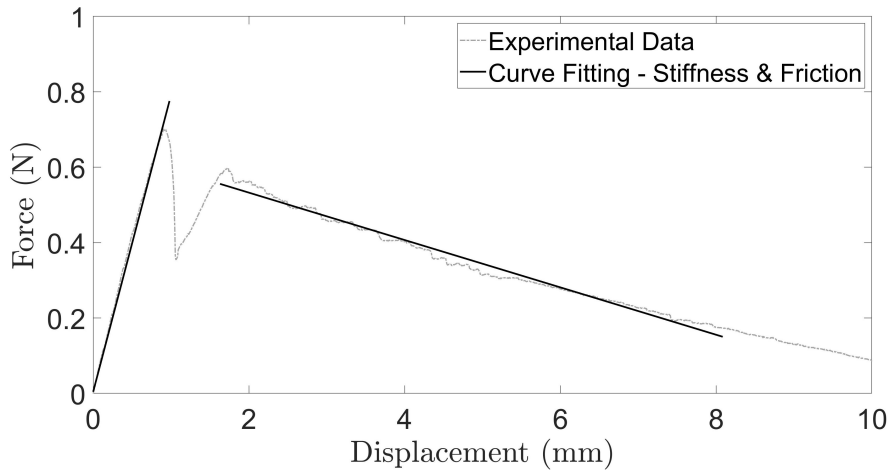


Figure 3.8.: Curve fitting example of a force-displacement diagram.

Two main areas get analyzed in this process. At the initial part of the diagram, until the highest point at which the debonding between fiber and elastomer matrix occurs, the first line is drawn for curve-fitting. This line is necessary for the correct evaluation of the main parameter of interest, the stiffness. It can be calculated by Equation 2.11. To be able to analyze the frictional behavior of the diagram, a second line must be placed over the diagram. In most cases it shows a negative behavior and is associated to the fiber being pulled-out of the elastomer matrix.

3.3.2. Overview of Experimental Data

Every elastomer and fiber has its specific properties. The combination of both materials therefore offers a very extensive range of different properties, which in some cases are desirable or must be avoided. Since there is not every data set shown in this chapter, Appendix A contains every single data set of the Single Fiber Pull-Out Tests conducted in Appendix A.1, Appendix A.2, and Appendix A.3. The data is evaluated with the source code shown in Appendix B. Figure 3.9 shows the results of the low material conducted without UV-light and the different fibers. The experiment's results of the respective fiber are averaged in Figure 3.9. The difference in magnitude of F_{\max} and also the difference in slope in the linear range until F_{\max} , which is associated with the stiffness k is clearly visible.

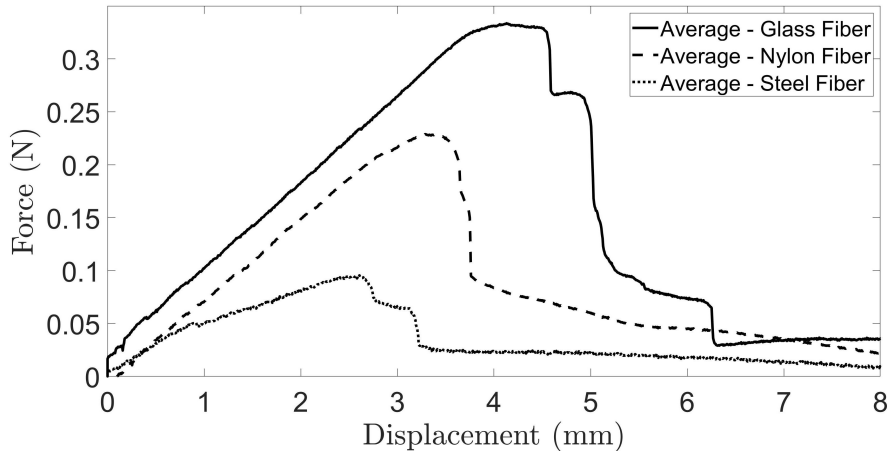


Figure 3.9.: Force-displacement diagram - low material - different fibers.

The highest stiffnesses can be seen with the glass and nylon fiber. These fibers have almost identical slopes and therefore nearly the same stiffness of 0.080 N mm^{-1} and 0.081 N mm^{-1} , only F_{\max} is smaller for the nylon fiber. This provides information about the strong adhesion between the low material and the glass fiber. A significantly flatter slope is associated with the steel fiber. The stiffness for the combination of the low material and steel fiber is around one third smaller compared to the other fibers with 0.048 N mm^{-1} . These tests are all conducted with the absence of UV-light. Interestingly, the composite materials used in these experiments can have completely different results and properties by introducing UV-light. Considerable changes of the composite material's behavior, in particular the low material with the glass fiber, can be seen in Figure 3.10. In this figure, the averaged values of the Single Fiber Pull-Out Tests without UV-light are compared with the results obtained under UV-illumination and different intensities, therefore the solid line with the highest value of F_{\max} is exactly the same as in Figure 3.9.

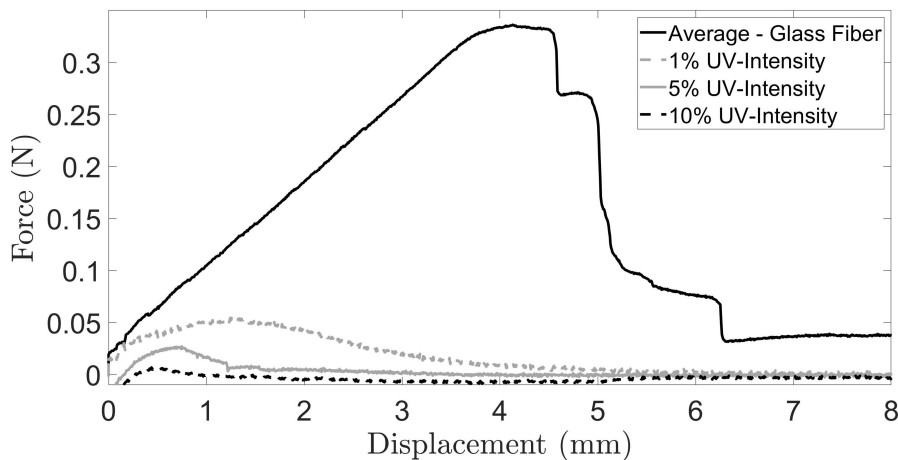


Figure 3.10.: Force-displacement diagram - low material - different UV-intensities.

By exposing the exact same composite material to UV-light, drastic changes can be rec-

ognized. Starting with the dashed, gray line in Figure 3.10, which shows the composite material's behavior under 1% UV-intensity, a drop of F_{\max} by a factor of seven can be noticed. Besides this drop, a major flattening of the slope is detected. The same trend is also valid for the composite material when illuminated with an intensity of 5% (solid gray line) and 10%. In this case, higher intensities lead to a higher drop of F_{\max} and to a decreasing trend of the slope and therefore stiffness. Specifically, the change in stiffness in Figure 3.10 has the following values: A drop in stiffness to 0.067 N mm^{-1} is noticed under 1% 0.063 N mm^{-1} under 5% and 0.060 N mm^{-1} under 10% UV-intensity. F_{\max} drops from 0.340 N at the absence of UV-light to 0.050 N, 0.025 N, and 0.010 N, respectively.

Now, the behavior of an elastomer material in combination with different fibers excluding UV-illumination is known. Moreover, the results of a composite material under varying UV-intensities are also known. Nevertheless, the illumination with UV-light does not necessarily mean a decrease of F_{\max} and the stiffness. It can also be the case that the respective values have no decrease at all, a small decrease, or even an increase. Figure 3.11 and Figure 3.12 show these cases. In Figure 3.11, the combination's behavior without UV-illumination between the three materials and the glass fiber are shown.

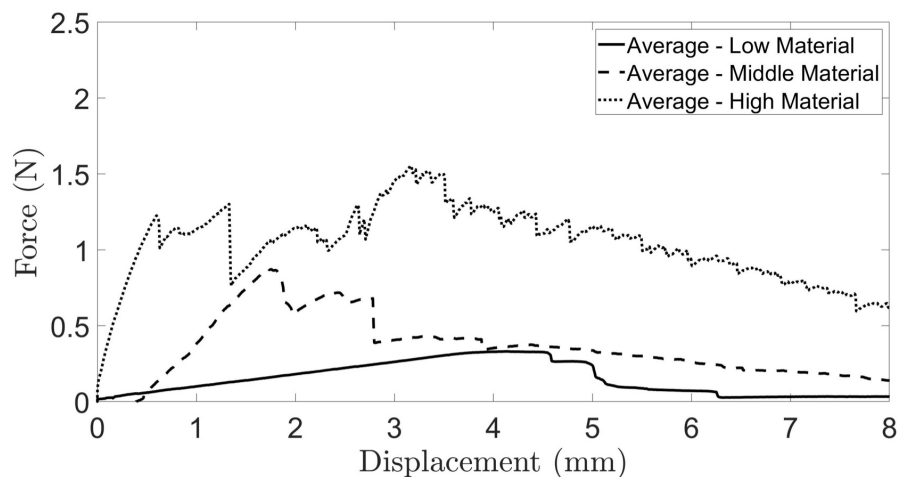


Figure 3.11.: Force-displacement diagram - different materials - glass fiber.

Clearly to be seen are the different magnitudes of F_{\max} and the various slopes of the corresponding composites, where the high material has the highest values and steepest slope down to the low material with the smallest values of F_{\max} and flattest slope corresponding to the stiffness.

The considerable differences under UV-illumination are shown in Figure 3.12. For a better comparison, only averaged values are used. The variation in UV-intensities gives each material the chance to show its behavior in case it requires different intensities to be activated.

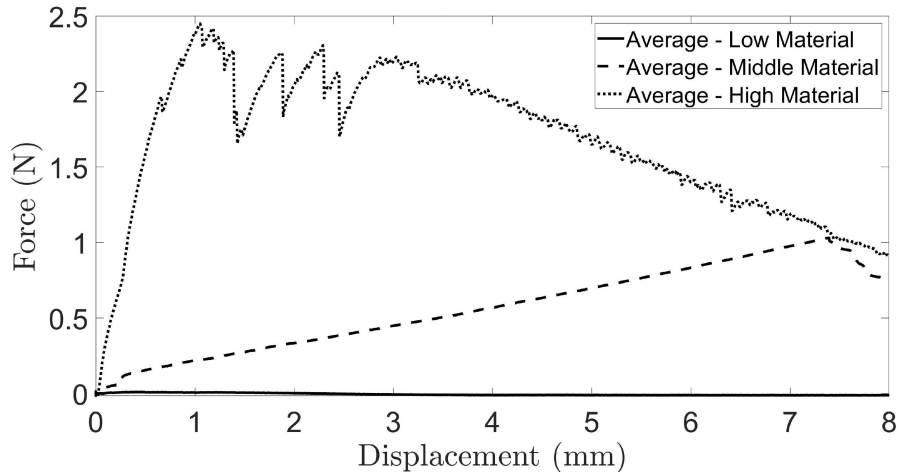


Figure 3.12.: Force-displacement diagram - different materials - glass fiber - UV.

This involves an increase of F_{\max} from approximately 1.50 N to 2.50 N and an increase in stiffness from 2.77 N mm^{-1} to 2.97 N mm^{-1} . A reason for an increase can be the polymerization of the composite material's chemical structure due to curing effects under UV-light. The middle material undergoes a relaxation under UV-light. The big change in stiffness from 0.75 N mm^{-1} to 0.13 N mm^{-1} is remarkable. As described previously, the low material also undergoes a decrease in F_{\max} and stiffness that tend to go towards zero.

The results and effects of the Single Fiber Pull-Out Tests are now known. To give an overview of the stiffness data collected in these experiments, Table 3.6 shows all results of the Single Fiber Pull-Out Tests. Table 3.6 illustrates the composite materials, the averaged data of the experiments without UV-light influence and the respective data for the different UV-intensities.

Table 3.6.: Stiffness Values - Single Fiber Pull-Out Test

| Composite Material | Stiffness Values / N mm^{-1} | | | |
|-------------------------|---------------------------------------|--------|--------|---------|
| | Avg. No UV | UV 1 % | UV 5 % | UV 10 % |
| Low Material & Steel | 0.048 | 0.032 | 0.005 | 0.098 |
| Middle Material & Steel | 0.882 | 1.018 | 1.157 | 1.409 |
| High Material & Steel | 1.305 | 1.474 | 1.507 | 1.129 |
| Low Material & Glass | 0.080 | 0.067 | 0.063 | 0.060 |
| Middle Material & Glass | 0.751 | 0.161 | 0.095 | 0.133 |
| High Material & Glass | 2.772 | 3.218 | 3.225 | 2.464 |
| Low Material & Nylon | 0.081 | 0.021 | 0.029 | 0.019 |
| Middle Material & Nylon | 0.736 | 0.414 | 0.067 | 0.113 |
| High Material & Nylon | 2.617 | 1.497 | 1.945 | 2.794 |

3.3.3. Interpretation of Results

In order to find the best composite material for the VSD, the stiffness values have to be interpreted correctly. The most important factor to be considered is the ratio between

the stiffness value without UV-illumination compared to the value with UV-illumination, which can be calculated as

$$\Psi = \frac{\text{Stiffness } UV_{Off}}{\text{Stiffness } UV_{On}} \quad (3.1)$$

and gives a better information about the reactive behavior of the composite material. By calculating all stiffness ratios Ψ , a heat-map is created that provides an overview and comparison between the different values, shown in Figure 3.13. The source code for the heat-map is shown in Appendix B.2. The rows show all the different fibers used in the experiments, and the columns are associated with the elastomer materials. Furthermore, the darker the rectangle in the heat-map, the bigger is the stiffness ratio and if it is smaller, it becomes brighter. The range of the ratio lies between zero and six, whereas the highest change between the UV-Off and UV-On state is characterized by the value six.

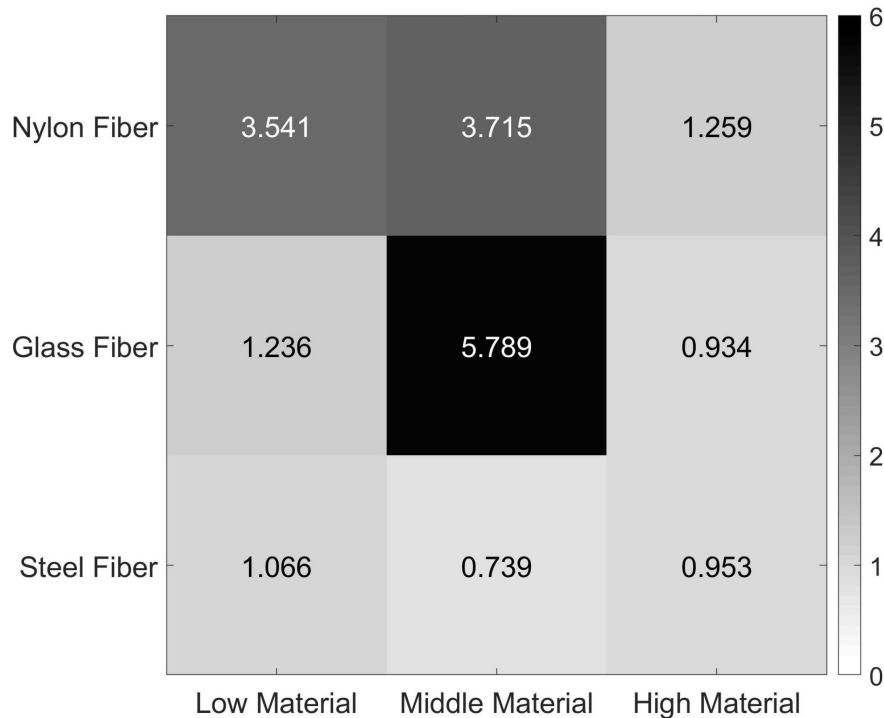


Figure 3.13.: Heat-map of the stiffness ratios Ψ .

As can be seen in Figure 3.13, the biggest ratios occur at the glass- and nylon fiber in combination with the low- and middle material. Especially the nylon fiber shows high ratio values for the just mentioned combinations. The glass fiber shows decent behavior with the low material and the highest ratio of all composites in combination with the middle material. Considering the steel fiber, a very small decrease in stiffness can be seen with the low material, whereas with the two other materials the opposite effect takes place.

3.3.4. Preliminary Material Selection for the Variable Stiffness Device

By precisely evaluating the results obtained from Figure 3.13, a pre-material selection for the VSD can be fulfilled. Therefore, one fiber and one material get eliminated from the wider selection. By taking into account the poor performance of the steel fiber combinations, this composite material is eliminated and will no longer be considered in the material selection process. Moreover, the glass- and nylon fiber in combination with the high material are also removed from the material selection process. Even though the ratio of the high material and nylon fiber shows a good performance, the high material becomes too brittle under UV-illumination and cannot be used as a VSD. Considering these facts, another type of experiment, the Three-Point Beam Test, is conducted with the glass- and nylon fiber in combination with the low- and middle material and will be discussed in Chapter 4.

4. Three-Point Beam Test

4.1. Composite Materials Used for Testing

4.1.1. Options and Properties of Composite Materials

To further specify the VSD's pre-material selection for a suitable composite material, another test procedure must be carried out: the Three-Point Beam Test. This test procedure is intended to provide more information about the composite materials and their real behavior when being exposed to external loads and UV-illumination. The composite materials investigated in this experiment are the four options previously defined in Chapter 3.3.4:

- Low Material & Glass Fiber
- Low Material & Nylon Fiber
- Middle Material & Glass Fiber
- Middle Material & Nylon Fiber

All of those materials show promising stiffness ratios and click-wise switching of their state under UV-light. To get an insight into the different forms of behavior of the beams, one fiber density (FD) is chosen prior to using others. For this case, a FD of 10 % is used. After conducting these experiments and choosing the composite material with the most feasible results, the experiment is conducted with three FDs to further investigate the composite. The FDs in this case are: 5 % , 10 % and 20 % Finally, a comparison between the three results is made and the final material selection for the VSD-prototype can be made.

4.1.2. Manufacturing Procedure of the Composite Materials

The manufacturing procedure for the test samples is done with the mold shown in Figure 4.1. It is manufactured by 3D-printing and consists of a UV-light resistant Polyactide (*PLA*).

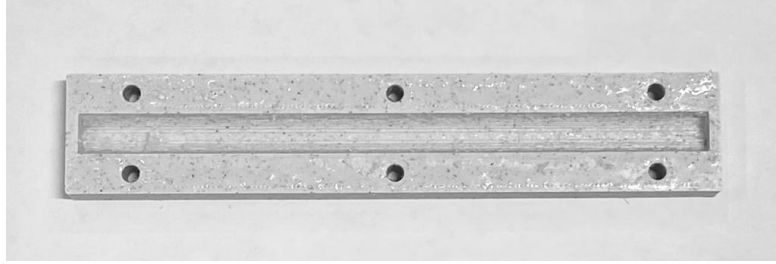


Figure 4.1.: Beam mold for the three-point beam test.

The annealed glass- or nylon fibers are put into this mold. Before putting them into the mold the amount of fibers corresponding to the FD must be determined. After this step the corresponding elastomer material is poured over the fibers up to the desired fill level. When the desired fibers and elastomer materials are in the mold, the mold is put into a vacuum chamber for at least 30 min in order to release all the air bubbles out of the elastomer. This step is crucial for the consistency and therefore the reliability of the beams behavior and the results. The next thing to do is to cure the composite material, as shown in Figure 4.2, in the mold. For this, a UV-light curing chamber filled with nitrogen gas is used and the composite material is cured for 200 s.

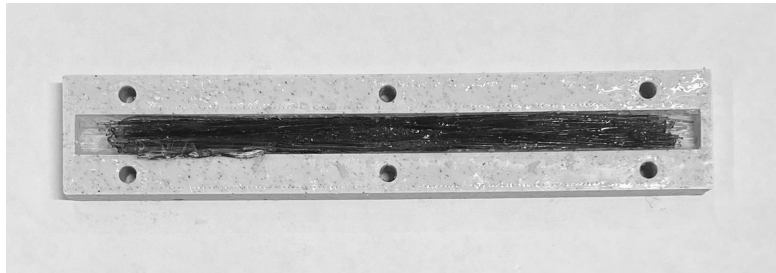


Figure 4.2.: Composite material in the beam mold.

By curing the beam for 200 s, a proper and solid state is reached. Now the beam can be taken out of the mold gently in order to cure the beam on the other side as well. For this side a curing time of 100 s is enough. At the end of all those steps the final beam and test sample looks like the one in Figure 4.3.

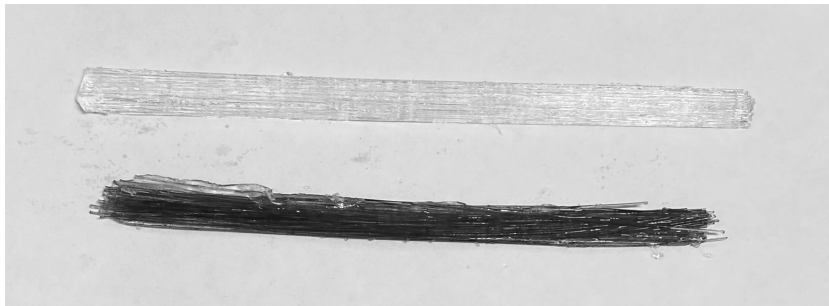


Figure 4.3.: Glass- and nylon fiber beam.

The upper beam is reinforced with optical glass fibers that are capable of carrying UV-light better, the lower beam consists of nylon fibers.

4.2. Experimental Setup for the Three-Point Beam Test

4.2.1. Testing Apparatus for the Three-Point Beam Test

The front view of the testing apparatus is illustrated in Figure 4.4. The main component of the experimental setup is the INSTRON® 6800 Series. It enables the penetration of the sample with the indenter and also processes the data of the results. On the right side of the INSTRON® 6800 Series, the Omnicure® S2000 is placed. This device is responsible for the UV-illumination during the UV-light experiments. The glass-tube can be adjusted and placed to the desired location on the test sample. Moreover, the timer for the correct illumination duration and the intensity can be directly set on the Omnicure® S2000. As a load-cell a 100 N load-cell from INSTRON® is used. It enables the right resolution for the processing of the data. If a higher valued load-cell were to be used, the force-displacement diagram would be too noisy for evaluation and the data could not be utilized. Due to the dangers of UV-illumination, the experimental setup must be completely enclosed. Therefore, non permeable acrylic for UV-light is installed and enclosing the setup, shown in Figure 4.4. It ensures that no direct contact with skin or eyes occurs.



Figure 4.4.: Three-point beam test setup - front view (left) & enclosed view (right).

Figure 4.5 shows the close view of the roller on the top, the composite beam made with nylon fibers, and the supports the beam is placed on.



Figure 4.5.: Three-point beam test setup - beam and supports.

Most importantly here is the correct alignment of the beam on the supports. Moreover, the roller must act on the exact center of the beam. Otherwise, the results may become invalid due to non-symmetric deflections of the beam. By preparing the setup like this, the results are saved in Excel[®] to be further evaluated in MATLAB[®].

4.2.2. Test Parameters for the Three-Point Beam Test

The parameters are listed in Table 4.1. For the Three-Point Beam Test, two different versions in terms of test parameters are conducted. The first experiments are carried out to become accustomed to the material behavior of the different composite beams (glass- and nylon fiber) which have a FD of 10%. It is important to mention that there may be small deviations in FDs due to the manufacturing process which can be neglected. All fibers have a diameter of 0.5 mm.

Table 4.1.: Test Parameters of the Three-Point Beam Tests

| Experiment | Displacement / mm | Velocity / mm min ⁻¹ | UV-Intensity / % |
|----------------------------|-------------------|---------------------------------|------------------|
| 1 st Experiment | 1.0 | 1.0 | 15.0 |
| 2 nd Experiment | 0.8 | 0.8 | 10.0 |

For the second experiment FDs of 5 %, 10 %, and 20 % are used. In these experiments however, only composite beams made of glass fibers are investigated due to the reasons that are explained in Chapter 4.3. The UV-light is turned at a displacement of 0.4 mm and turned off when the displacement reaches the same displacement in the backward movement. For the experiments without UV-illumination, the whole test is deflected until 0.8 mm and then relaxed to its original position. A slightly smaller displacement, velocity, and UV-intensity is used for the second experiment. This is done because of the increase in quality of the data due to the time the composite beam has to adapt. Each experiment is conducted only once.

4.3. Results and Data of the Three-Point Beam Test

The results of the Three-Point Beam Tests are used for the final material selection to find an appropriate material used in the VSD-Prototype. To achieve this, the corresponding stiffness values must be analyzed in the same way by curve-fitting as described in Chapter 3.3.1 for the Single Fiber Pull-Out Tests. By obtaining this information, the most fitting characteristics can be analyzed easily and finally be implemented in the VSD-Prototype.

4.3.1. Analysis of Force-Displacement Diagrams

Figure 4.6 illustrates the results for the nylon-reinforced beams with different elastomers, under UV-illumination, and without. The first Three-Point Beam Tests are conducted with the nylon-reinforced beams. All of the beams have the same FD and therefore also the test parameters for the first type of experiment are valid here.

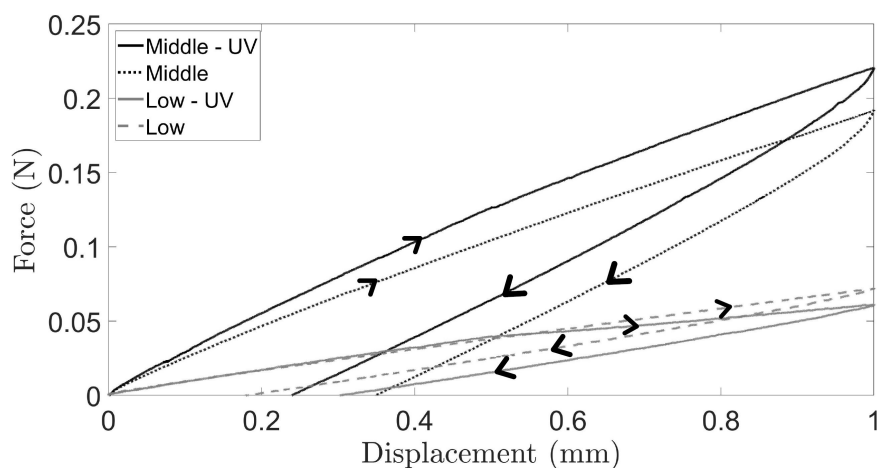


Figure 4.6.: Nylon fiber - overlap.

Starting with the investigation of the middle material, the steepest slope can be seen at the middle material under UV-illumination. It has the highest stiffness value of

0.22 N mm^{-1} and the highest force of 0.22 N . Comparing these results with the test conducted without UV-illumination, a smaller stiffness can be perceived. In this case a stiffness value of 0.19 N mm^{-1} and correspondingly a force of 0.22 N is valid. Logically, this behavior is not desired for the VSD-prototype. Therefore, this material is no longer considered in the material-selection process. Looking at the low material, a higher stiffness can be determined for the beam without UV-illumination compared to the beam with UV-illumination. Stiffness values of 0.08 N mm^{-1} for the case of the non-illuminated beam and 0.06 N mm^{-1} for the illuminated one are valid and show the desired drop in stiffness when shining UV-light on the sample. Noticeable changes in behavior can be seen with the glass-reinforced beams. In Figure 4.7, significantly higher stiffnesses are measured for both the middle- and low materials. By taking a closer look at the middle material, an almost identical behavior and stiffness of 4.42 N mm^{-1} without UV-light and 4.50 N mm^{-1} with UV-light can be noticed. This fact confirms that the middle material is not suitable for a VSD, no matter with which fiber it is reinforced.

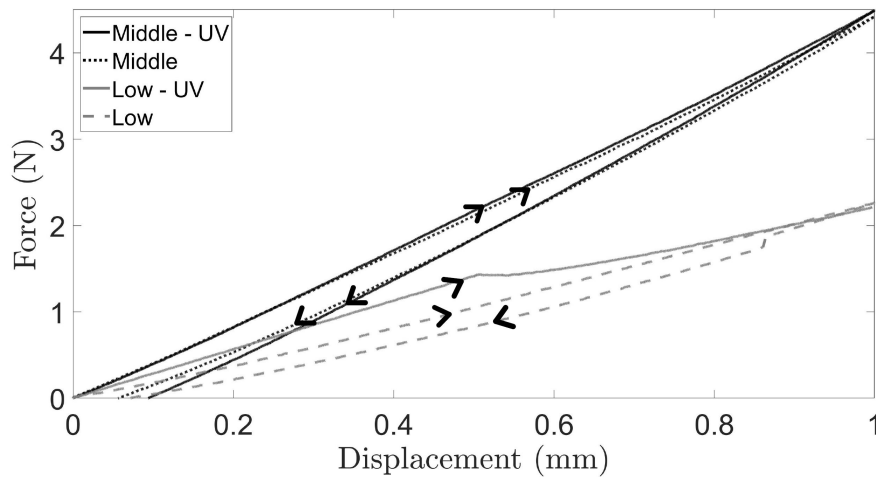


Figure 4.7.: Glass fiber - overlap.

Comparing the middle material to the low material, not only a smaller stiffness of 2.25 N mm^{-1} but also a change in slope and stiffness to 1.59 N mm^{-1} when illuminating the glass-reinforced beam can be noticed. The change in slope at 0.5 mm is the point of interest and must be investigated in more experiments. Due to an error in the saving process the low material under UV-light only shows half a cycle, which is no problem because of the obvious reaction to UV-light at the rising slope. By selecting the low material in combination with the glass fibers as the composite material to be further investigated, six more experiments are carried out to gain more knowledge about its behavior. For these experiments the test parameters for the second experiment of Table 4.1 are used and the percentages in Figure 4.8 present the various (glass) FDs of the beams. The gray areas in the bottom subplots indicate the area where the UV-illumination is present.

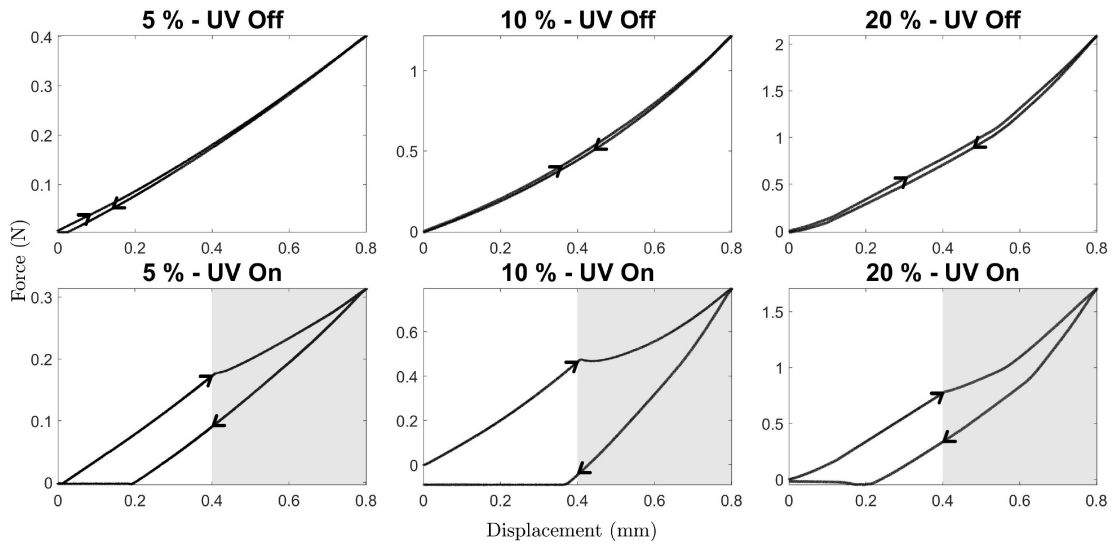


Figure 4.8.: Glass fiber - different densities - UV on / off.

Starting with the top-left plot in Figure 4.8, a stiffness value of 0.51 N mm^{-1} and a maximum force of 0.4 N acts. It is noteworthy that for this and the case of 10% FD, almost zero energy is dissipated during the loading and relaxation phase (the energy is the area between the rising and the falling lines that are nearly identical). An increase of stiffness is subject to both the 10% and 20% beams that are 1.53 N mm^{-1} and 2.61 N mm^{-1} . The highest forces are 1.22 N and 2.09 N respectively. Also, with the beam of 20% FD, only very little energy is dissipated during loading and relaxation. A significant difference is noticeable for all three UV-light experiments. For the case of 5% FD a total drop of 0.16 N , for 10% of 0.73 N , and for 20% a total drop of 0.3 N is observed. As can be derived from Figure 4.8, the highest energy dissipation is in the case of the 20% FD beam. Examining the various ratios Ψ , as well as the real performances, is now subject of the final material selection.

4.3.2. Examination and Interpretation of the Collected Data

The correct interpretation of the collected data is the crucial part for the final material selection of the VSD-prototype. In order to choose a well performing composite material however, not only the stiffness values and Ψ are to be considered, but also the real-life handling (fluid/solid/sticky behavior; manufacturing possibilities and convenience of the composite beam; etc.). Table 4.2 illustrates the total difference Δ and Ψ conducted from the Three-Point Beam Tests.

Table 4.2.: Stiffness Difference & Ratio - Three-Point Beam Test

| Composite Material | Total Difference Δ | Stiffness Ratio Ψ |
|--------------------------------|---------------------------|------------------------|
| Low Material & Glass (10 %) | -0.66 | 1.42 |
| Middle Material & Glass (10 %) | 0.08 | 0.98 |
| Low Material & Nylon (10 %) | -0.02 | 1.33 |
| Middle Material & Nylon (10 %) | 0.03 | 0.86 |
| Low Material & Glass (5 %) | -0.16 | 1.45 |
| Low Material & Glass (10 %) | -0.73 | 1.91 |
| Low Material & Glass (20 %) | -0.30 | 1.12 |

At first glance it seems to be the best choice to take the composite material with the highest ratio Ψ . It is definitely a good start but as just mentioned, there are also other factors that have to be taken into account. One of the most important things during the material selection process besides the stiffness (ratio) is the transmission of the UV-light through the beam. In the case of nylon fibers, only very little transmittance of UV-light can be seen. This is due to a mix of high scattering and non-permeability of the respective fibers. On the other hand, glass fibers show a very good and reliable transmission-behavior for UV-light. Another factor is the brittleness of the materials where the middle material acts very brittle, especially under long duration of UV-illumination. In addition, the stiffness values for the nylon-reinforced composites are too low for a meaningful application. This is the reason why the main focus lies on the low material and the glass fibers. In order to be on the shortlist, rather high values of Δ and Ψ have to be present.

4.3.3. Final Material Selection for the Variable Stiffness Device-Prototype

With the help of the fundamental preparations in the material selection process made in Chapter 3 and Chapter 4, a final material selection for the VSD-prototype can be made. In addition to the various results obtained, also personal experiences are integrated into the selection process. This is the reason why finally the following material is chosen for being used in the VSD-prototype: Low Material & Glass Fiber with 20 % FD. The specific composite material shows the best overall performance for the specific application in terms of Δ and Ψ . This composition tends to be very easy to be manufactured and also does not demonstrate too sticky or too fluid behavior under ambient conditions. Also, repetitive using of the material is possible and wear is kept very low. Additionally, the selected composite material shows the force ranges that are needed to withstand certain loads and to meet some boundary conditions. Even though the comparable composites beams with different FDs show higher values of Δ and Ψ , they do not tend to be feasible for high loads and are therefore not taken into account.

5. Design and Manufacturing of a VSD-Prototype

5.1. Design Objective of the Prototype and Methodology

5.1.1. Design Concept and Requirements of the Prototype

Many different possibilities for designing a VSD-prototype exist. Starting with gloves, lifting-devices, and lifting-supports, a useful application can be seen in a medical-technological device like an endoscope. Therefore, the design and implementation of a VSD-endoscope is pursued. It is supposed to be stiff during operational work at the desired location and soft when actuating and moving the device. Repeatability and accuracy are an essential part that must work indispensably. The main idea behind the VSD-prototype concept is to convert a stiff, beam-like actuator to an adjustable, modifiable, and finally, soft actuator. One of the most important requirements for the prototype is the actuator's response time, which has to be in a range of 1 s. In concrete terms this means that by turning on the UV-light, the actuator gets soft and when turning the UV-light off, the actuator becomes stiff again and back to its original state. It does not matter in which configuration of shape the actuator's beam is in this case, therefore, arbitrary shapes can be achieved with this design concept. Other crucial requirements for the prototype are the high repeatability of its processes, the minimization of wear, high safety standards, and the ability to control the various movements of the actuator. High repeatability and minimization of wear, is shown through the ability to undergo the process from a stiff-state to a soft-state and vice versa various times, as well as the unrestricted ability to move and bend the actuator. For safety reasons, under no circumstances there must not be glass shattering no matter how much the prototype is bent. If the glass fibers shatter inside the actuator, a certain probability exists of glass shards exiting the actuator and injuring the patient; an event which must never occur.

5.1.2. Key Features and Functions

Special actuators need specific features as well as functions. As mentioned before, mainly four key features and functions of the VSD-prototype exist:

- Rapid Stiffness Changes

- Arbitrary Shaping
- High Repeatability
- High Safety Standards

To make this possible, some essential components must be part of the VSD-prototype such as the OmniCure[®] S2000 which is controlling the stiffness by UV-illumination. Nylon-wires are used for the movement of the endoscope by surrounding the actuator's beam and by respective pulling. An optical lens which is focusing the UV-light on the actuating beam in the base shown in Figure 5.4. This is the interface of the OmniCure[®] S2000 and the actuator beam. All these components must work hand in hand to ensure the correct actuation. It is crucial that the actuator's beam has the correct fibers embedded and in the correct volume fraction with the elastomer material. This enables slower or faster actuation times and defines the stiffness of the actuator's beam.

5.1.3. Technical drawings of the Variable Stiffness Device-Prototype

For the assembly of the VSD-prototype, three main parts have to work together. The main movement is done by the actuator's beam itself; the nylon-wires just define the direction of movement. The main components are:

- Prototype Base
- Actuator Beam
- Movement Clamps

The top-view on the base is depicted in Figure 5.1. It is used for the assembly of the actuator beam and the OmniCure[®] S2000 which activates the desired stiffness change. For this, on the wider side with the 13 mm opening, the OmniCure[®] S2000 tube is fixed flush to the optical lens located at the constriction. The actuator beam is coming from the other side. It is also fixed flush with the optical lens which in further consequence transmits the light into the beam. The four holes with a diameter of 6.20 mm are necessary to fix the base on the experimental setup's plate.

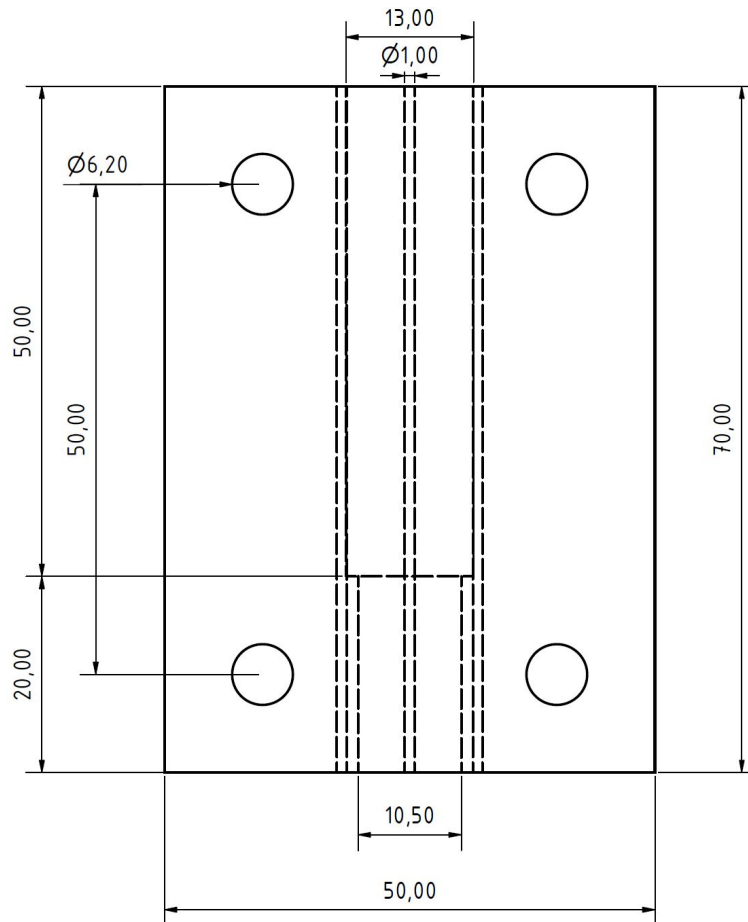


Figure 5.1.: Prototype base - top view.

A front view of the base is shown in Figure 5.2 showing the guidance holes of the wires.

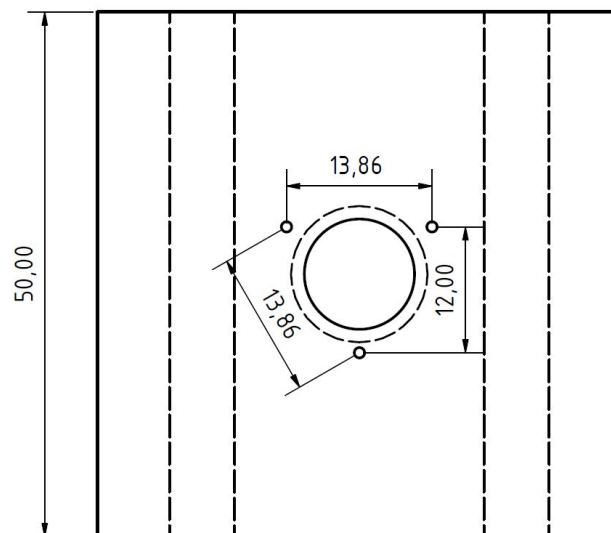


Figure 5.2.: Prototype base - front view.

These holes are arranged in an equilateral triangle to ensure the uniform movement

control of the beam and endoscope respectively. The wires go completely through the base to the side of the OmniCure[®] S2000. There they can be operated by simply pulling them on the requested side to enable the movement of the endoscope. At the beam itself, the wires are fixed by the movement clamps shown in Figure 5.3.

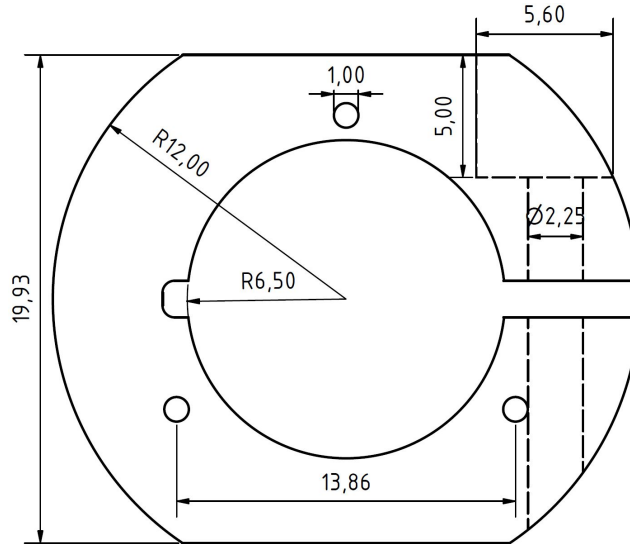


Figure 5.3.: Movement clamp - front view.

The movement clamps are then uniformly arranged along the beam at a distance of 3 cm. The beam is at the inside of the clamp and the tightness can be adjusted by the screw in the right part of the drawing in Figure 5.3. Again, the holes for the wires are arranged in an equilateral triangle for uniform movement. For the sake of convenience, Figure 5.4 shows the angular view of the prototype base.

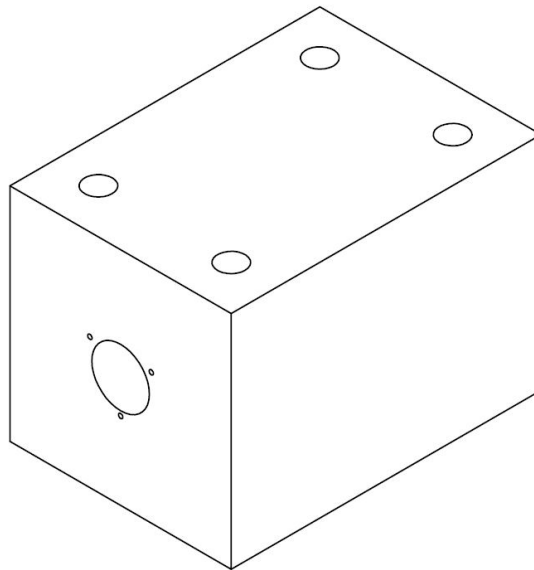


Figure 5.4.: Prototype base - angular view.

5.2. Actuation and Real Setup of the VSD-Prototype

Figure 5.5 shows the actuator's beam attached to the base, without the movement clamps and wires. The main actuation of the VSD-prototype is carried out by the OmniCure[®] S2000. By the illumination of the actuator's beam, the reaction of the elastomer material is activated and so the softening, as well as stiffness change is fulfilled.

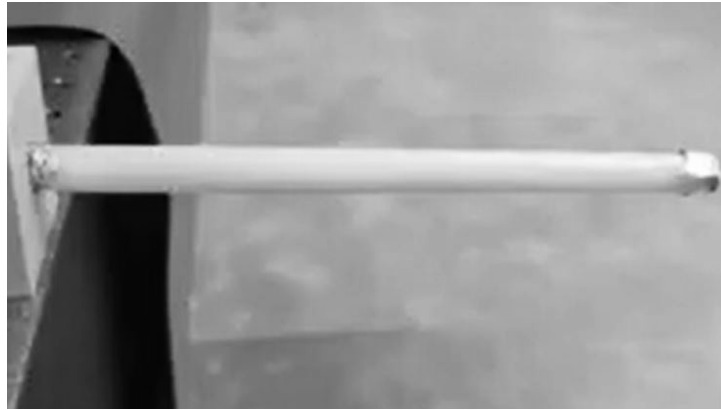


Figure 5.5.: Prototype base & beam - side view.

The beam is very stiff in its initial shape in the absence of UV-light as can be seen in Figure 5.5. For the first try of the real actuation behavior, weights with either 100 g or 200 g are used to deflect the beam and show the change in displacement more obviously. For the UV-intensity a magnitude of 10 % is used with a illumination duration of 10 s and 15 s respectively. As mentioned in Chapter 4.3.3, a FD of 20 % is used for the beam. Because of delivery problems, the fiber composition must be slightly modified and therefore a ratio of 50/50 with optical glass- and PMMA fibers is used. The characteristics of both fibers, especially in transmission of (UV)-light are very similar which make the modification tolerable. Besides that, small modification are made for the elastomer material. Specifically, Zirconium(IV)-oxide (ZrO_2) powder with 99 % metal basis is added to the low material. The addition of this powder does not influence the mechanical characteristics of the material but the transmission behavior of the UV-light. Respectively, the added material improves the scattering behavior of the beam due to its better refractive index and helps to distribute the UV-light in the entire beam. In Figure 5.6, the actuator is shown with its initial displacement initiated by a weight of 100 g. This weight helps to emphasize and to better show the reaction of the composite material under UV-illumination.



Figure 5.6.: Prototype base & beam with weight - side view.

By the addition of 100 g, the beam bends but is still stiff and stable. The goal of the proof of concept is a weight drop due to the decrease in stiffness of the beam when activated with UV-light. The beam should remain in the position which it held at the moment of shutting down the UV-light. This step is intended to be performed numerous times before the composite material, especially the elastomer component, becomes worn out. The illuminated VSD-prototype can be seen in Figure 5.7.



Figure 5.7.: Prototype base & beam illuminated - side view.

After initiating UV-illumination, the elastomer material reacts to it and a decrease in stiffness results. The embedded fibers transmit the UV-light longitudinally through the beam to the very end of the beam. With the help of ZrO_2 , scattering is increased and so is the reaction to the UV-light in all parts of the beam. By progressing UV-illumination, the beam becomes softer, and its tip starts to bend downwards to a maximum of approximately 1 cm. As a result, the weight either drops (Figure 5.8) or stays on the beam

with a displacement of approximately 1 cm in the case of this experiment. This proves the softening of the composite beam and the underlying concept. The displacement stays at the point where the UV-light is turned off and therefore shows the click-wise increase in stiffness under the absence of UV-light.



Figure 5.8.: Prototype base & beam deflected - side view.

5.3. Discussion of the Variable Stiffness Device-Prototype

There have been many interesting findings during the VSD-prototype phase. Some development plans work out the way they should, obviously though, there are also propositions that do not work out the way they are intended to. Starting with the successful aspects of the VSD-prototype: the stiffness and toughness of the entire beam show promising results and performances. These two behaviors are proven by the fact of a deformation that tends towards zero when putting weight on the beam, which proves the correct choice of composite material in the final material selection of Chapter 4.3.3. The overall performance in terms of bending ability without breaking of fibers give satisfying outcomes that must be further improved but are already on the right track. Moving over to the transmission behavior of the beam, adequate performance can be detected when under UV-illumination. It shows that the fibers propagate the UV-light adequately along the entire beam all the way to the tip of it. Improvements in the transmission behavior are made by the usage of optical fibers instead of conventional ones. Another improvement is reached by the addition of ZrO_2 to the low material. The scattering of the UV-light is significantly increased by said compound and emphasize in the activation of the low material. Prior to the addition of ZrO_2 , a gradient in transmission has been investigated and is gone due the modification. This gradient has the highest UV-exposure at the very beginning of the beam where it is in contact with the actuator's base and linearly decreases towards the tip of the beam.

Potential for improvements abounds for the present VSD-prototype. Starting with the manufacturing process of the beam, optimizations in embedding the fibers in the mold

for the beam are the first improvement to be made. As the VSD-prototype is now, non-perfectly aligned and distributed fibers can be found in the beam. With the help of a different process of embedding and distributing the fibers in the mold, more uniform behaviors in displacement and especially in the transmission behavior of UV-light can be achieved. With the winding technique, as it is done now, non-uniform lumps of fibers are present in the beam which lead to adequate behavior, but not perfect, transmission behavior. Breakage of the glass fibers occur regularly due to too high forces acting at the corners of the mold during the process. This leads to a waste of expensive fiber material, risk of injuries, and waste of time. Another point of improvement is the replacement of a heat shrink tubing with a material that does behave as solid. Because of the heat shrink tubing used in the VSD-prototype, valuable changes in stiffness are not being utilized due to the higher outer stiffness of the tubing. This restriction does not allow the composite material to reach its full adaption potential in stiffness and needs to be changed in order to see further improvements. In terms of manufacturing processes, a better setup for the extraction of air bubbles must be implemented. The current vacuum chambers work satisfactorily, nevertheless air bubbles still exist in the material and decrease the ability of transmission behavior and affect the mechanical properties of the actuator. The low material works fine in theory and shows a lot of the researched data proven in the application. Enhancing of transmission experiments and data have to be carried out which is the main problem why the actuator does not reach the stiffness change it should. More research must be done in the investigation of further polymerization of the low material under UV-light. This problem affects the mechanical characteristics of the composite material, and it wears out the material earlier than desired. To be able to correctly move the VSD-prototype, the movement clamps from Chapter 5.2 must be installed and tested properly. They could be actuated by several electric motors and regulated by a corresponding controller for smooth and accurate movements.

Finally, putting all the aspects together, a reliable VSD-endoscope can be developed. Further experiments, especially in the transmission of UV-light must be carried out inevitably to reach that goal. More time has to be invested into the composition of slightly modified elastomer materials in interaction with optical fibers in order to best prevent polymerization of the elastomer material in order to avoid high wear.

6. Summary and Outlook

6.1. Summary

In the various experiments concerning the design and manufacturing process of the VSD-prototype numerous valuable data sets are found. Starting with the Single Fiber Pull-Out Tests conducted in Chapter 3, new insights and areas of findings are made through this newly invented experimental setup and the experiments performed with this. The experiments show the interaction of special elastomer materials in combination with different fibers. These kinds of experiments in association with the special materials have never been carried out before and therefore gather completely new findings in research along this field of materials science and soft-robotics that can be now be furthered.

Referring to the findings conducted in relation to the VSD-prototype and the (preliminary) material selection process, promising results are collected and analyzed carefully before selecting a shortlist for further experiments. Before the selection of the shortlist, one must mention that some unknown factors exist which cannot be found about through the Single Fiber Pull-Out Tests directly. Some uncertainties would for example be the influence of polymerization under UV-illumination, the impact of different UV-intensities in relation to the activation ability of the CAN-materials, and the number of cycles the composite material can withstand before wearing out. Despite these uncertainties, the results provide solid information about the material behavior and fundamentally help in the material selection process and with the creation of the shortlist.

The second part in terms of experiments relates to the Three-Point Beam Tests and its final material selection for the VSD-prototype. Again, completely new insights in the field of the investigated composite materials are made since there have neither been similar experiments nor has there been any data gathered before. By this experiment, it can increase and broaden the findings conducted by the Single Fiber Pull-Out Tests due to the variation of fiber densities and UV-intensities. It must be mentioned that it can be realistically investigate the behavior of real composite beams by the Three-Point Beam Tests, which is not possible with the Single Fiber Pull-Out Tests. This fact drastically helps in the final material selection for the VSD-prototype and shows similar composite beams behaviors already in the testing phase. Another interesting finding are the changes in stiffness when illuminated by UV-light, as the drops in stiffness are closer to reality in this kind of experiment. The combination of the Single Fiber Pull-Out Tests and Three-Point Beam Tests verify the step-by-step material selection process from big

scale to the small scale and the final material selected, the low material reinforced by glass fibers.

Finally, the VSD-prototype is able to be produced after the careful material selection. Various findings can be seen again in the VSD-prototype and confirm the results and analysis of the previous work. Due to problems in delivery and manufacturing, a few points could not be investigated in the way they should have. A main issue is the improvisation and the adaption of *PMMA* fibers to the glass fibers in a ratio of 50/50. Even though the characteristics are acceptable, the full potential of the optical glass fibers is not exploited and leaves unanswered questions. Another problem is the movement controlling of the VSD-prototype. This point is not fully investigated, as the change in stiffness is shown with the addition of weights and the resulting deformation of the beam. Still, the proving of this concept can be considered as a success as can the material selection process in total. By involving further experiments and investigations such as the influence of polymerization under UV-light or the scattering of it, further improvements can be made and the VSD-prototype may be significantly improved.

6.2. Outlook

Although there are very promising approaches and results, several things must be improved in order to reach the goal of a proper working VSD-device. First, a broad spectrum of investigations must be conducted in order to gain more knowledge about the influence of polymerization in the Single Fiber Pull-Out Test, the Three-Point Beam Test, and the VSD-prototype. By doing this, the increase of stiffness can be bypassed when the UV-illumination is carried out for a longer duration of time (more than 20 s). This also helps in increasing the lifetime of the VSD-prototype and its elastomeric material since the wear out can be decreased significantly. The next big step in improving the VSD-prototype is to better the manufacturing process of the composite beam. The way it is constructed now, lumps of fibers are in the middle of the beam, and on the outer sides of the beam, there is mainly elastomeric material. This uneven distribution of fibers affects the scattering of the UV-light and is also the reason why the big drop in stiffness does not occur the way it should. A solution for this would be a vertical setup for evenly distributed fibers. After the distribution, a mold encloses the fibers and the elastomer material can be poured in from the top. It is important to mention that the mold must be transmissive to UV-light, otherwise the beam cannot be cured or used. With uniform UV-illumination, the scattering effects inside the beam can be investigated. As it is now, only assumptions can be made on the UV-light distribution and therefore it is important to do further research in this field. This would also be a chance to leave ZrO_2 out of the low material and allow it to stay in the original chemical composition. The last point that must be improved for the prototype case is to design a proper movement control. This can be done with the wire-guidance in a uniformly distributed triangle and could be actuated by a common position control that has an

easy setup and provides reliable actuation. The input for the actuation can be given by a stick and the user could easily control the VSD-prototype and guide it to go either left, right, up, or down. For the UV-illumination a switch can be installed that starts the reaction of the elastomer material click-wisely and stops it, when desired. When incorporating these points, a basic VSD-prototype can be manufactured and the fundamental functions can be proven and further investigated to further improve the abilities of the device and finally have a reliable and fully functional VSD.

Bibliography

- [1] M. Brancadoro, M. Mariangela, F. Grani, S. Tognarelli, A. Menciasci, and M. Cianchetti, "Toward a variable stiffness surgical manipulator based on fiber jamming transition," *Frontiers in Robotics and AI*, vol. 6, 2019.
- [2] D. Sadhan, *Rubber Technologies Handbook*, 1st ed. Croatia: IntechOpen, 1996.
- [3] M. Ashby, *Materials Selection in Mechanical Design*, 4th ed. Amsterdam: Elsevier Ltd., 2011.
- [4] T. Sabu, P. M. Visakh, M. Aji, and C. Arup, *Advances in Elastomers 2*, 2nd ed. Berlin Heidelberg: Springer, 2013.
- [5] H. Ferial, P. Alokesh, and B. Animesh, *Tribology of Elastomers*, 1st ed. Singapore: Springer, 2022.
- [6] M. Ashby and D. Jones, *Engineering Materials 2*, 3rd ed. Amsterdam: Elsevier Ltd., 2011.
- [7] G. Ehrenstein and S. Pongratz, *Resistance and stability of polymers*, 1st ed. Munich: Hanser Publishers, 2013.
- [8] N. Pazooch, B. Rouhollah, and A. Adloo, "Fabrication of semi-conductive natural rubber nanocomposites with low copper nanoparticle contents," *Elsevier Ltd.*, vol. 108, 2016.
- [9] Polymerdatabase, "Polymerdatabase Stress Strain Behavior of Polymers [Online]," Available: <https://polymerdatabase.com/polymer%20physics/Stress-Strain%20Behavior.html>, accessed: 14.04.2023.
- [10] M. S. Hoo Fatt and X. Ouyang, "The behavior of elastomers at high strain rates," *WIT Press*, vol. 87, 2006.
- [11] R. D. de Leon and L. Valencia, "Bioelastomers: current state of development," *Journal of Material Chemistry A*, 2022.
- [12] Freudenberg Forschungsdienste KG., *Elastomere Werkstoffe*, 1st ed. Weinheim: Eigenverlag, 2001.
- [13] M. Ashby and D. Jones, *Engineering Materials 1: An Introduction to Properties, Applications and Design*, 3rd ed. Amsterdam: Elsevier Ltd., 2005.
- [14] F.-J. Falkner, "Technische Mechanik 2," Lecture material, 2018, Management Center Innsbruck.

- [15] M. Ashby, H. Shercliff, and D. Cebon, *Engineering, Science, Processing and Design*, 3rd ed. Amsterdam: Elsevier Ltd., 2007.
- [16] D. Gross, W. Hauger, J. Schröder, W. Wall, and J. Bonet, *Engineering Mechanics 2: Mechanics of Materials*, 2nd ed. Berlin: Springer, 2007.
- [17] C. J. Kloxin, T. F. Scott, B. J. Adzima, and C. N. Bowman, "Covalent adaptable networks (CANs): A unique paradigm in cross-linked polymers," *Macromolecules*, vol. 43, 2010.
- [18] C. J. Kloxin and C. N. Bowman, "Covalent adaptable networks: smart, reconfigurable and responsive network systems," *Royal Chemical Society*, vol. 42, 2013.
- [19] K. Cheng, A. Chortos, A. L. Lewis, and D. R. Clarke, "Photoswitchable covalent adaptive networks based on thiolene elastomers," *ACS Applied Materials & Interfaces*, vol. 14, 2022.
- [20] C. Bowman, F. Du Prez, and J. Kalow, "Introduction to chemistry for covalent adaptable networks," *Royal Society of Chemistry*, vol. 11, 2020.
- [21] K. M. McBride, T. W. Worell, T. Brown, M. L. Cox, N. Sowan, C. Wang, M. Podgorski, M. A. Martinez, and C. N. Bowman, "Enabling applications of covalent adaptable networks," *Annual Review of Chemical and Biomolecular Engineering*, vol. 10, pp. 175–198, 2019.
- [22] S. B. Bonab, V. Karimkhani, and I. Manas-Zloczower, "Ultra-fast microwave assisted self-healing of covalent adaptive polyurethane networks with carbon nanotubes," *Macromolecular Materials and Engineering*, vol. 304, 2018.
- [23] H. Dodiuk, *Handbook of Thermoset Plastics*, 4th ed. Amsterdam: Elsevier Ltd., 2022.
- [24] A. Toncheva, L. Blanc, P. Dubois, and J.-M. Raquez, "Multi-responsive polymer actuators by thermo-reversible chemistry," *In Book: Mechanically Responsive Materials for Soft Robotics*, pp. 277–306, 2019.
- [25] C. Wang, "Fracture mechanics of single-fibre pull-out test," *Journals of Materials Science*, vol. 32, 1997.
- [26] C. Y. Yue and W. L. Cheung, "The interfacial properties of fibrous composites, part 2: Determination of interracial shear strength, interracial coefficient of friction, and the shrinkage pressure on the fibre," *Journals of Materials Science*, vol. 27, 1992.
- [27] C. K. Y. Leung and V. C. Li, "New strength-based model for the debonding of discontinuous fibres in an elastic matrix," *Journals of Materials Science*, vol. 26, 1991.
- [28] L. Teuber, H. Fischer, and N. Graupner, "Single fibre pull-out test versus short beam shear test: comparing different methods to assess the interfacial shear strength," *Journals of Materials Science*, vol. 48, 2013.

- [29] C. Y. Yue and W. L. Cheung, "The interfacial properties of fibrous composites, part 3: Effect of the thickness of the silane coupling agent," *Journals of Materials Science*, vol. 29, 1994.
- [30] C. DiFrancia, T. Ward, and R. Claus, "The single-fibre pull-out test. 1: Review and interpretation," *Composites Part A: Applied Science and Manufacturing*, vol. 27, pp. 597–612, 1996.
- [31] Y. Tian and L. Guo, "Adhesion performance of uhmwpe fiber treated with polyethylene wax grafted methyl methacrylate alone or in conjunction with silane coupling agent," *Journal of Adhesion Science and Technology*, vol. 35, 2021.
- [32] Z. Baohua, L. Daxiang, and S. Huaizhi, "Single pullout experiment and reinforcement properties of basalt fiber in vegetation concrete," *Scientific reports*, vol. 12, 2022.
- [33] M. R. Piggott, "The single-fibre pull-out method: its advantages, interpretation and experimental realization," *Composite Interfaces*, vol. 1, 1993.
- [34] C. L. Victor, W. Cynthia, W. Shuxin, O. Atsuhisa, and S. Tadashi, "Interface tailoring for strain-hardening polyvinyl alcohol-engineered cementitious composite (pva-ecc)," *ACI Materials Journal*, vol. 99, 2002.
- [35] D. D. Scărlătescu, A. Modrea, and M. D. Stanciu, "Three-point bend test to determine the mechanical behavior of the tubes used in water supply networks," *Procedia Manufacturing*, vol. 32, pp. 179–186, 2019.
- [36] F. Mujika, "On the effect of shear and local deformation in three-point bending tests," *Polymer Testing*, vol. 26, pp. 869–877, 2007.
- [37] S. J. Jalali and F. Taheri, "A new test method for measuring the longitudinal and shear moduli of fiber reinforced composites," *Journal of Composite Materials*, vol. 33, pp. 2134–2160, 1999.
- [38] H. Imamura, K. Kadooka, and M. Taya, "A variable stiffness dielectric elastomer actuator based on electrostatic chucking," *Soft matter*, vol. 13, 2017.
- [39] S. Wolf, G. Grioli, O. Eiberger, W. Friedl, M. Grebenstein, H. Hoppner, E. Burdet, D. G. Caldwell, R. Carloni, M. G. Catalano, D. Lefeber, St. Stramigioli, N. Tsagarakis, M. van Damme, R. van Ham, B. Vanderborght, L. C. Visser, A. Bicchi, and A. Albu-Schaffer, "Variable stiffness actuators: Review on design and components," *IEEE/ASME Transactions on Mechatronics*, vol. 21, 2016.
- [40] L. Wang and Y. Yang, Y. Chen, C. Majidi, F. Iida, E. Askounis, and Q. Pei, "Controllable and reversible tuning of material rigidity for robot applications," *Materials Today*, vol. 21, 2018.
- [41] J. Shintake, B. Schubert, S. Rosset, H. Shea, and D. Floreano, "Variable stiffness actuator for soft robotics using dielectric elastomer and low-melting-point alloy," pp. 1097–1102, 2015.

- [42] B. Vanderborght, A. Albu-Schaeffer, A. Bicchi, E. Burdet, D. G. Caldwell, R. Carloni, M. Catalano, O. Eiberger, W. Friedl, G. Ganesh, M. Garabini, M. Grebenstein, G. Grioli, S. Haddadin, H. Hoppner, A. Jafari, M. Laffranchi, D. Lefeber, F. Petit, S. Stramigioli, N. Tsagarakis, M. van Damme, R. van Ham, L. C. Visser, and S. Wolf, "Variable impedance actuators: A review," *Robotics and Autonomous Systems*, vol. 61, 2013.
- [43] J. Kwon, I. Choi, M. Park, J. Moon, B. Jeong, P. Pathak, J. Ahn, and Y. L. Park, "Selectively stiffening garments enabled by cellular composites," *Advanced Materials Technologies*, vol. 7, 2022.
- [44] Futek Advanced Sensor Technology, Model LSB200 Datasheet, "Low Capacity Miniature S-Beam Jr. Load Cell [Online]," accessed: 15.06.2023.

List of Figures

| | | |
|------|--|----|
| 1.1 | VSD as an endoscope | 2 |
| 2.1 | Six families of materials science | 4 |
| 2.2 | Molecular structure of an elastomer | 6 |
| 2.3 | Cross-linked elastomers in original and deformed state | 6 |
| 2.4 | Stress-strain curves of polymers | 7 |
| 2.5 | Applications of elastomers | 8 |
| 2.6 | Definition of strain by u-x diagram | 9 |
| 2.7 | Stress-strain curve of a polymer material | 10 |
| 2.8 | Schematic structure of photo-activated CAN elastomers | 13 |
| 2.9 | Shape morphing device made of a CAN | 14 |
| 2.10 | Basic structure of the single fiber pull-out test | 15 |
| 2.11 | Different stages during a single fiber pull-out test | 16 |
| 2.12 | Force-displacement diagram of a valid & invalid single fiber pull-out test | 16 |
| 2.13 | Schematics of a basic three-point beam test | 19 |
| 2.14 | Basic force-displacement curve of a three-point beam test | 20 |
| 2.15 | Variable stiffness device with electrical actuation | 21 |
| 3.1 | Side-view of the test mold | 24 |
| 3.2 | Top-view of the test mold | 25 |
| 3.3 | Front-view of the test mold | 26 |
| 3.4 | Empty test mold | 27 |
| 3.5 | Filled test mold | 28 |
| 3.6 | Complete test mold | 28 |
| 3.7 | Final experimental setup | 29 |
| 3.8 | Curve fitting example of a force-displacement diagram | 31 |
| 3.9 | Force-displacement diagram - low material - different fibers | 32 |
| 3.10 | Force-displacement diagram - low material - different UV-intensities | 32 |
| 3.11 | Force-displacement diagram - different materials - glass fiber | 33 |
| 3.12 | Force-displacement diagram - different materials - glass fiber - UV | 34 |
| 3.13 | Heat-map of the stiffness ratios Ψ | 35 |
| 4.1 | Beam mold for the three-point beam test | 38 |
| 4.2 | Composite material in the beam mold | 38 |
| 4.3 | Glass- and nylon fiber beam | 38 |
| 4.4 | Three-point beam test setup - front view & enclosed view | 39 |

| | | |
|-----|---|----|
| 4.5 | Three-point beam test setup - beam and supports | 40 |
| 4.6 | Nylon fiber - overlap | 41 |
| 4.7 | Glass fiber - overlap | 42 |
| 4.8 | Glass fiber - different densities - UV on / off | 43 |
| 5.1 | Prototype base - top view | 47 |
| 5.2 | Prototype base - front view | 47 |
| 5.3 | Movement clamp - front view | 48 |
| 5.4 | Prototype base - angular view | 48 |
| 5.5 | Prototype base & beam - side view | 49 |
| 5.6 | Prototype base & beam with weight - side view | 50 |
| 5.7 | Prototype base & beam illuminated - side view | 50 |
| 5.8 | Prototype base & beam deflected - side view | 51 |

List of Tables

| | | |
|-----|--|----|
| 3.1 | Elastomer and Fiber Materials used in the Single Fiber Pull-Out Tests . | 23 |
| 3.2 | Characteristics of the Elastomers used in the Single Fiber Pull-Out Tests | 23 |
| 3.3 | Characteristics of the Fibers used in the Single Fiber Pull-Out Test . . . | 24 |
| 3.4 | Test Parameters - Single Fiber Pull-Out Test | 26 |
| 3.5 | Experiment Composition of the Single Fiber Pull-Out Tests | 30 |
| 3.6 | Stiffness Values - Single Fiber Pull-Out Test | 34 |
| 4.1 | Test Parameters of the Three-Point Beam Tests | 40 |
| 4.2 | Stiffness Difference & Ratio - Three-Point Beam Test | 44 |

List of Symbols

| Symbol | Name | Unit |
|--------------|----------------------------------|--------------------|
| A | Area of the plain | m^2 |
| F | Force | N |
| G | Shear-modulus | N m^{-2} |
| σ | Stress | N mm^{-1} |
| u | Displacement | mm |
| ϵ | Strain | – |
| l | Length | mm |
| T | Temperature | $^{\circ}\text{C}$ |
| E | Modulus of elasticity | N m^{-2} |
| τ | Interfacial shear strength | N mm^{-1} |
| d | Diameter | mm |
| R | Radius of matrix | mm |
| r | Radius of fiber | mm |
| V | Electrical voltage | V |
| p | Pressure | N mm^{-1} |
| Ψ | Stiffness ratio | – |
| FD | Fiber density | % |
| T_g | Glass transition temperature | $^{\circ}\text{C}$ |
| ΔT | Temperature difference | $^{\circ}\text{C}$ |
| σ_y | Yield stress | N mm^{-1} |
| α_T | Coefficient of thermal expansion | K^{-1} |
| ϵ_T | Thermal strain | – |
| F_{\max} | Maximum force | N |
| E_f | Young's modulus of fiber | N m^{-2} |
| E_m | Young's modulus of matrix | N m^{-2} |
| Δ | Total Difference | – |

Abbreviations

| | |
|------------------|---------------------------|
| ZnO | Zinc oxide |
| H | Hydrogen |
| CH ₃ | Methanide |
| Cl | Chlorine |
| e.g. | exempli gratia |
| CAN | Covalent adaptive network |
| PDMS | Polydimethylsiloxane |
| etc. | et cetera |
| VSD | Variable Stiffness Device |
| UV | Ultraviolet |
| C | Celsius |
| VHB | Very High Bond |
| Avg. | Average |
| PLA | Polyactide |
| ZrO ₂ | Zirconium(IV)-oxide |

A. Detailed Measurement Results – Single Fiber Pull-Out Test

As there are averaged results and overlaps used for the sake of convenience in Chapter 3, not all results are able to be investigated on their own and need to be shown for transparency. In the following figures, the corresponding results for the glass fibers, nylon fibers and steel fibers are shown. To repeat, each of the fibers is tested three times without UV-light and three times under UV-light and changing UV-intensities. It is important to mention that the axes may slightly differ from figure to figure due to better visibility and the fact that forces change drastically when changing material compositions.

The following Chapters A.1, A.2, and A.3 show the subsequent figures:

- Glass Fibers in Chapter A.1: Figure A.1, Figure A.2, and Figure A.3
- Steel Fibers in Chapter A.2: Figure A.4, Figure A.5, and Figure A.6
- Nylon Fibers in Chapter A.3: Figure A.7, Figure A.8, and Figure A.9

By comparing the stiffness values and just the form of the graphs, the repeatability and consistency can be approved. Therefore it is also able to approve the method of using this test method for obtaining comparable results in the process of a fundamental material selection.

A.1. Single Fiber Pull-Out Test – Glass Fiber

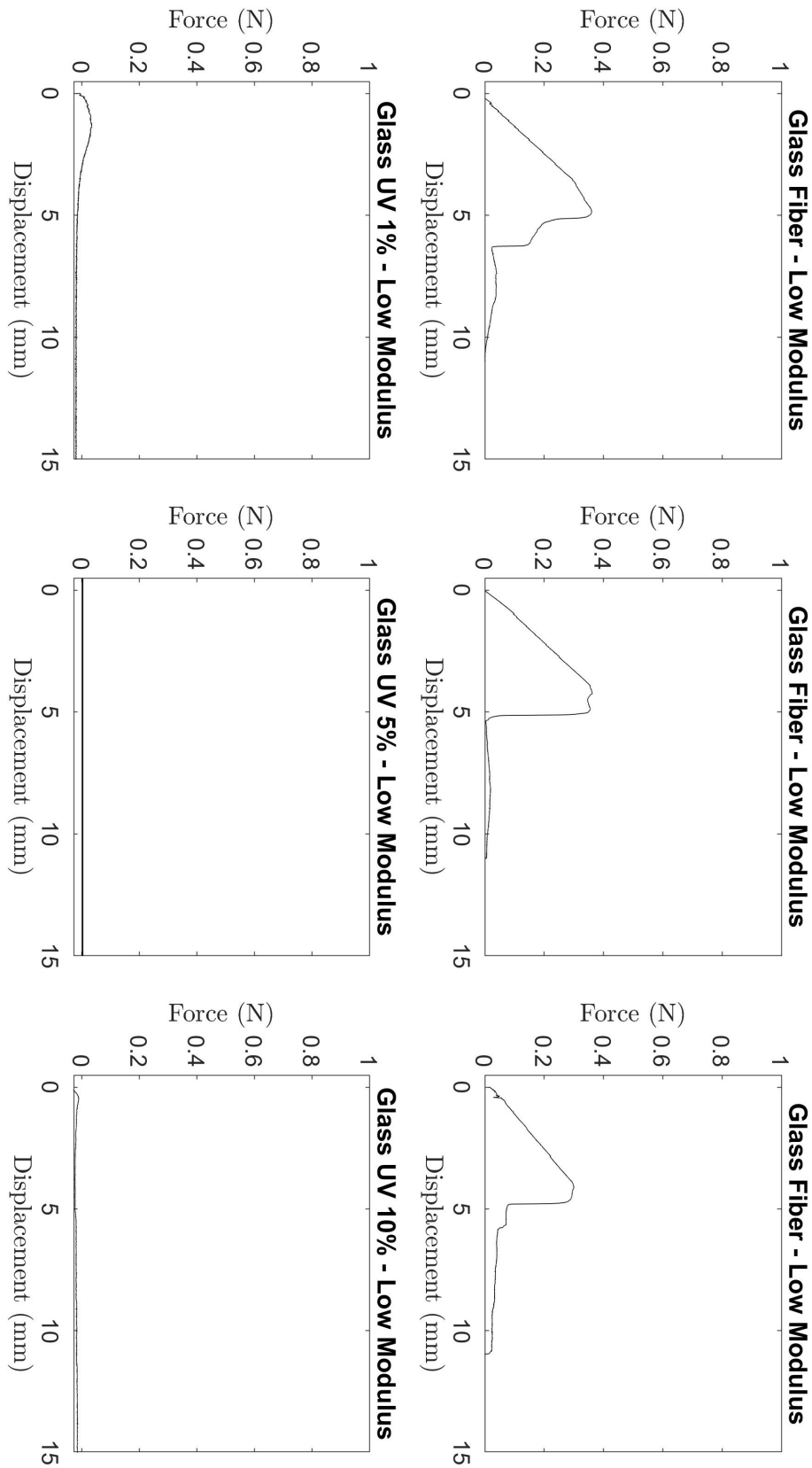


Figure A.1.: Detailed measurement results – glass fiber & low material.

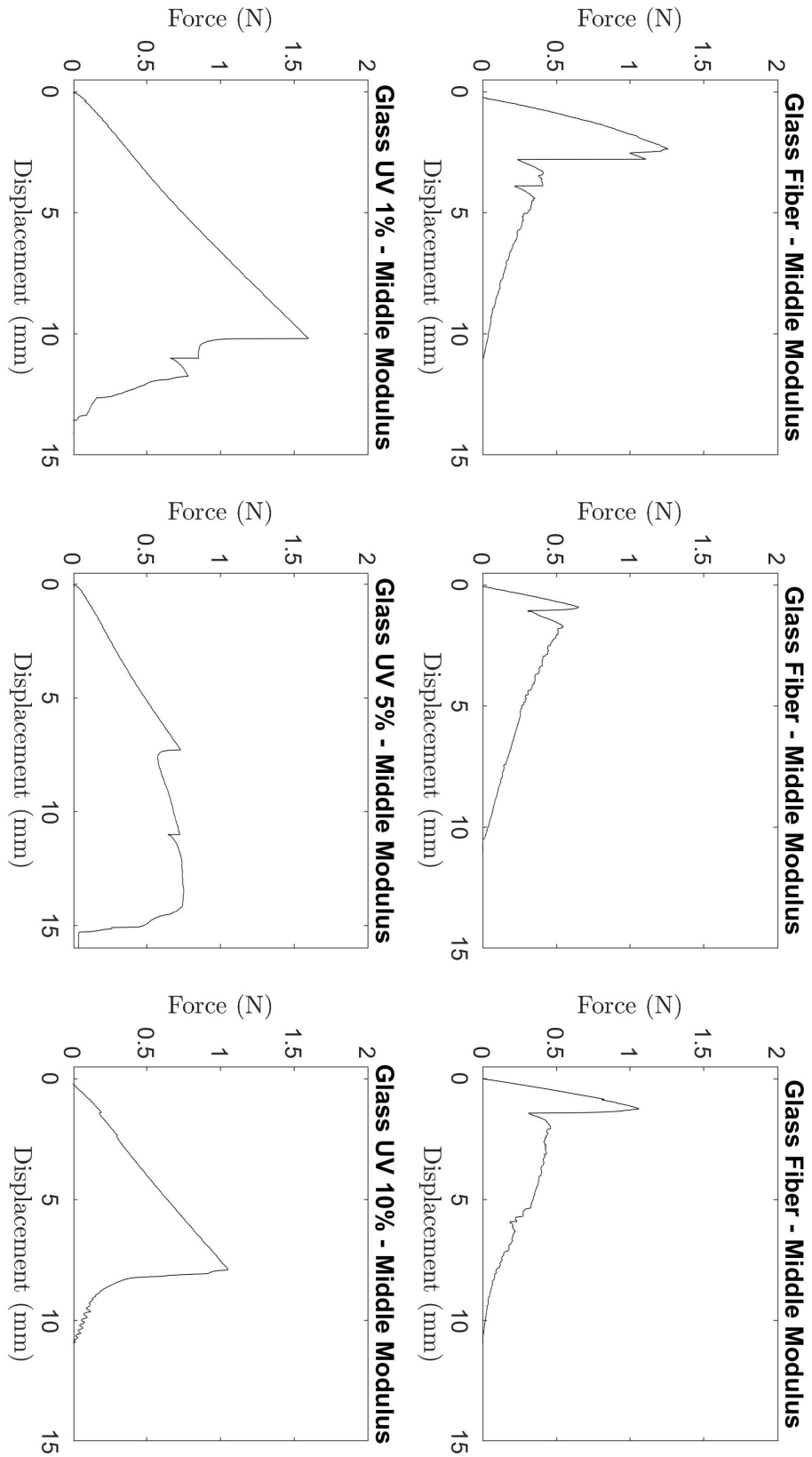


Figure A.2.: Detailed measurement results – glass Fiber & middle material.

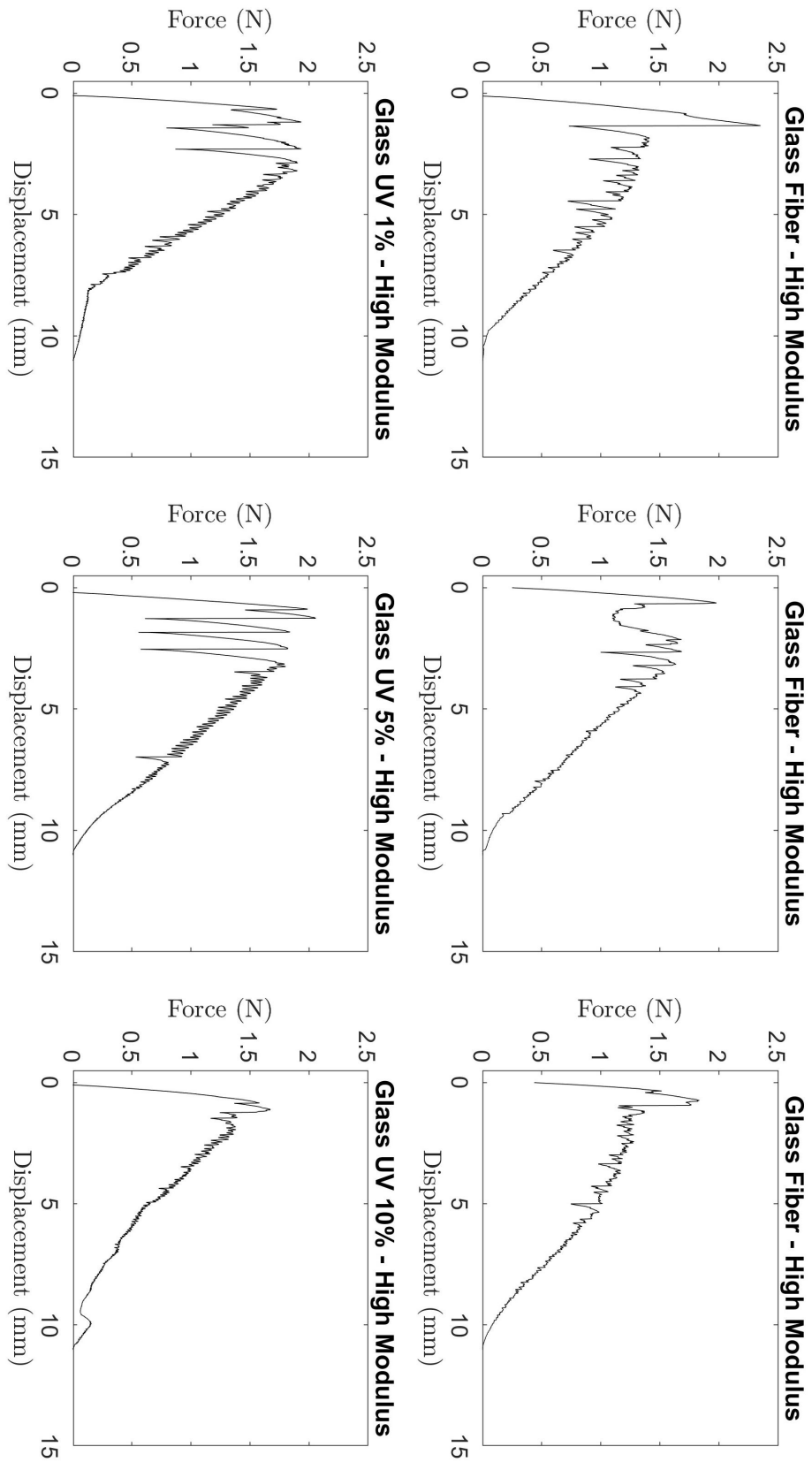


Figure A.3.: Detailed measurement results – glass fiber & high material.

A.2. Single Fiber Pull-Out Test – Steel Fiber

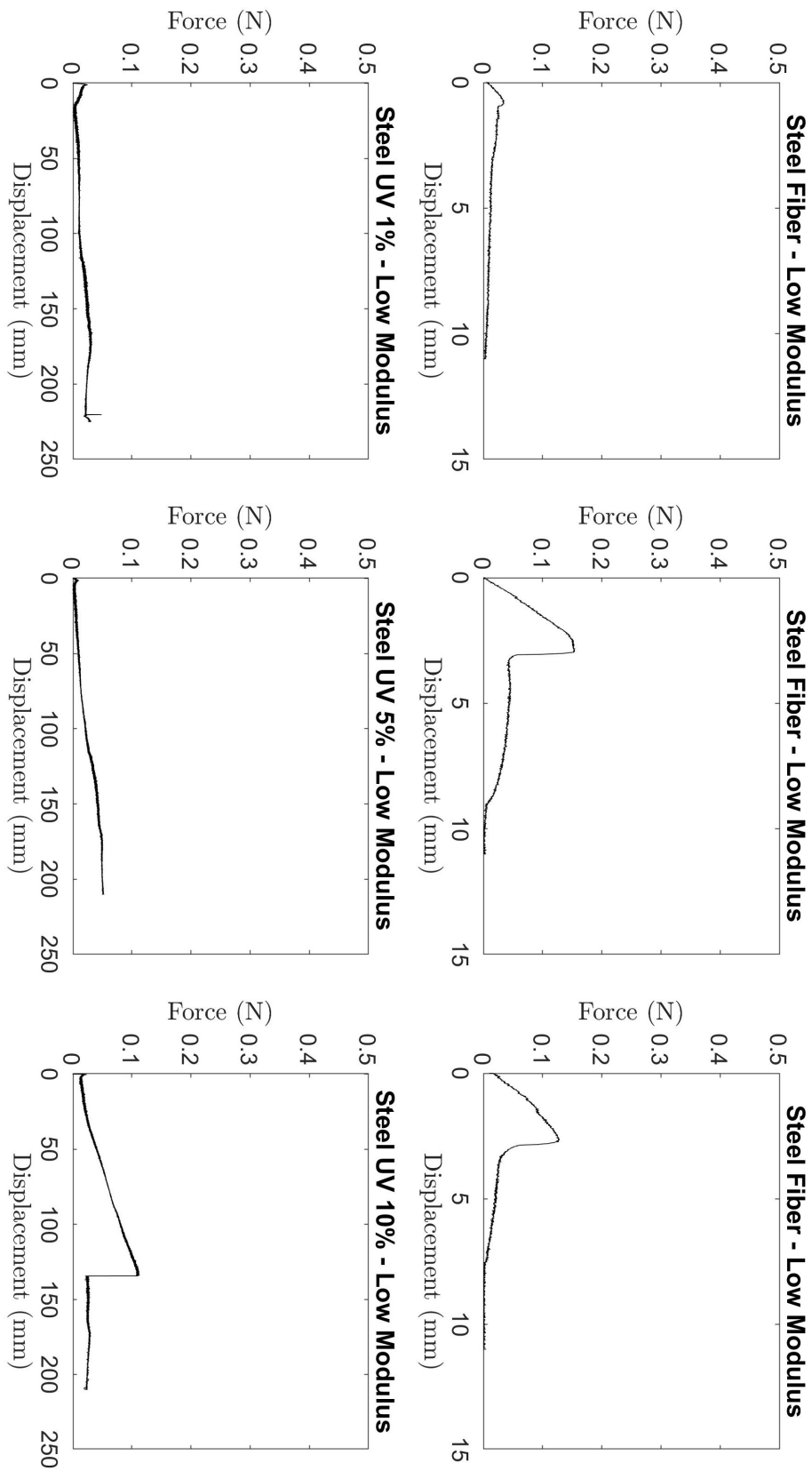


Figure A.4.: Detailed measurement results – steel fiber & low material.

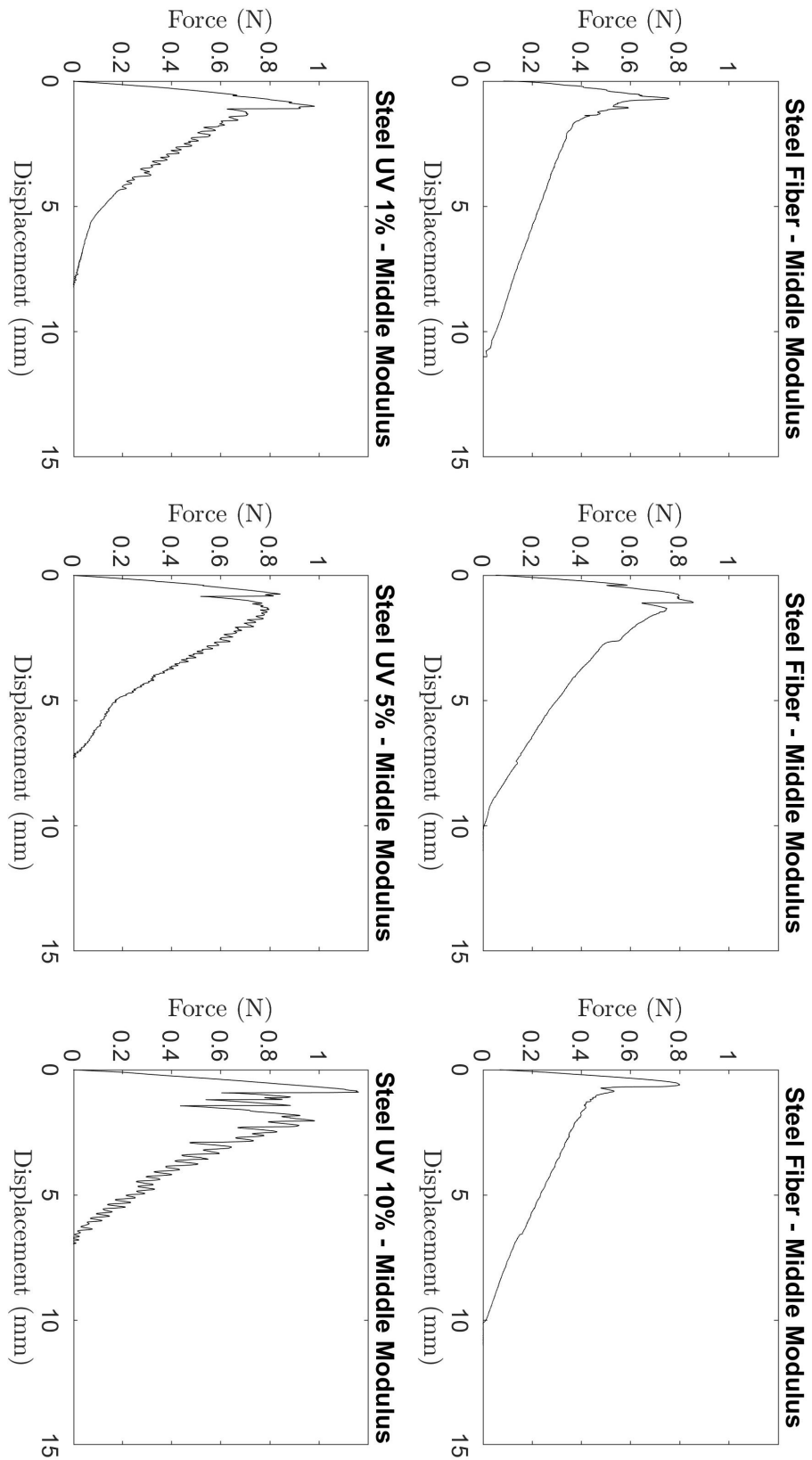


Figure A.5.: Detailed measurement results – steel fiber & middle material.

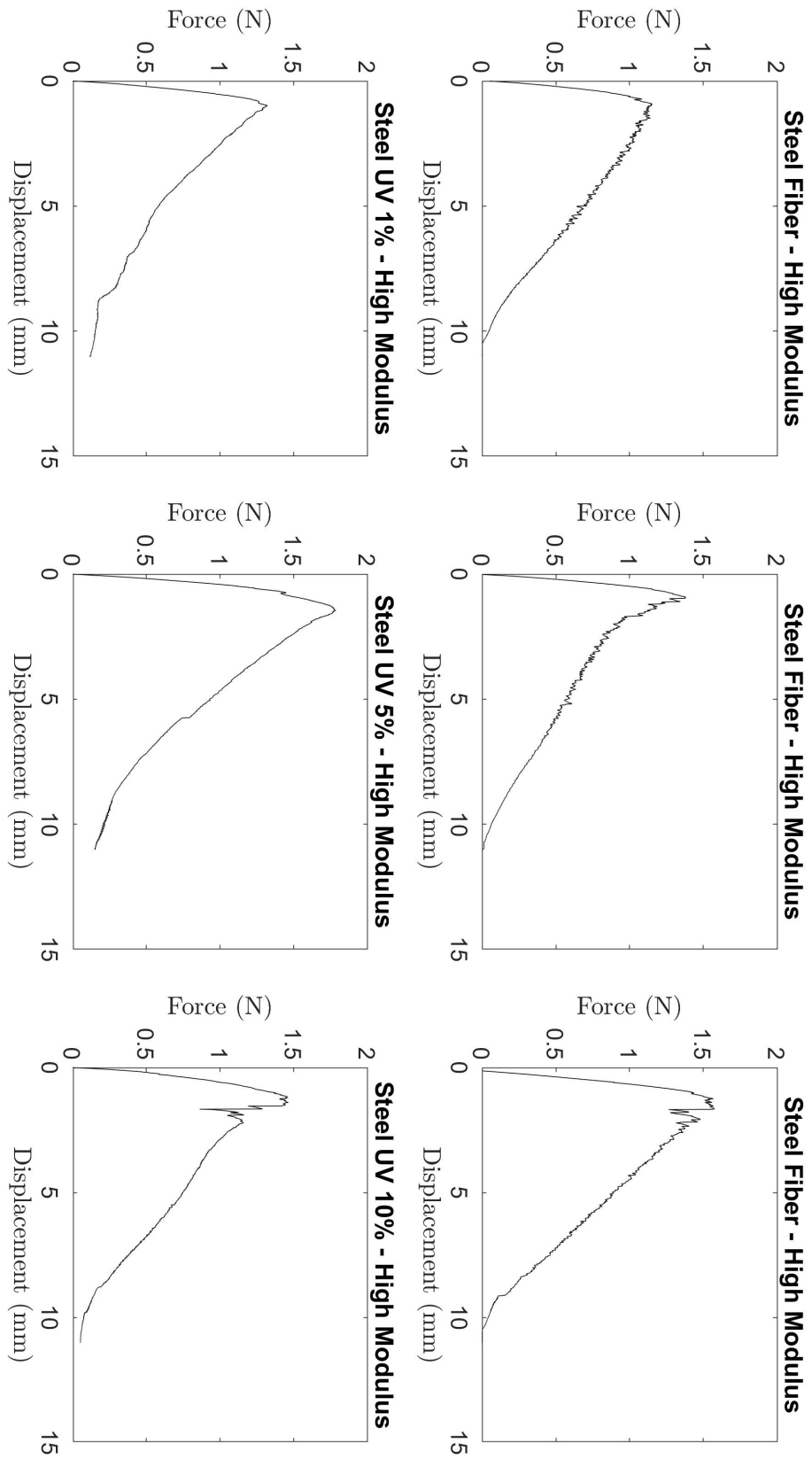


Figure A.6.: Detailed measurement results – steel fiber & high material.

A.3. Single Fiber Pull-Out Test – Nylon Fiber

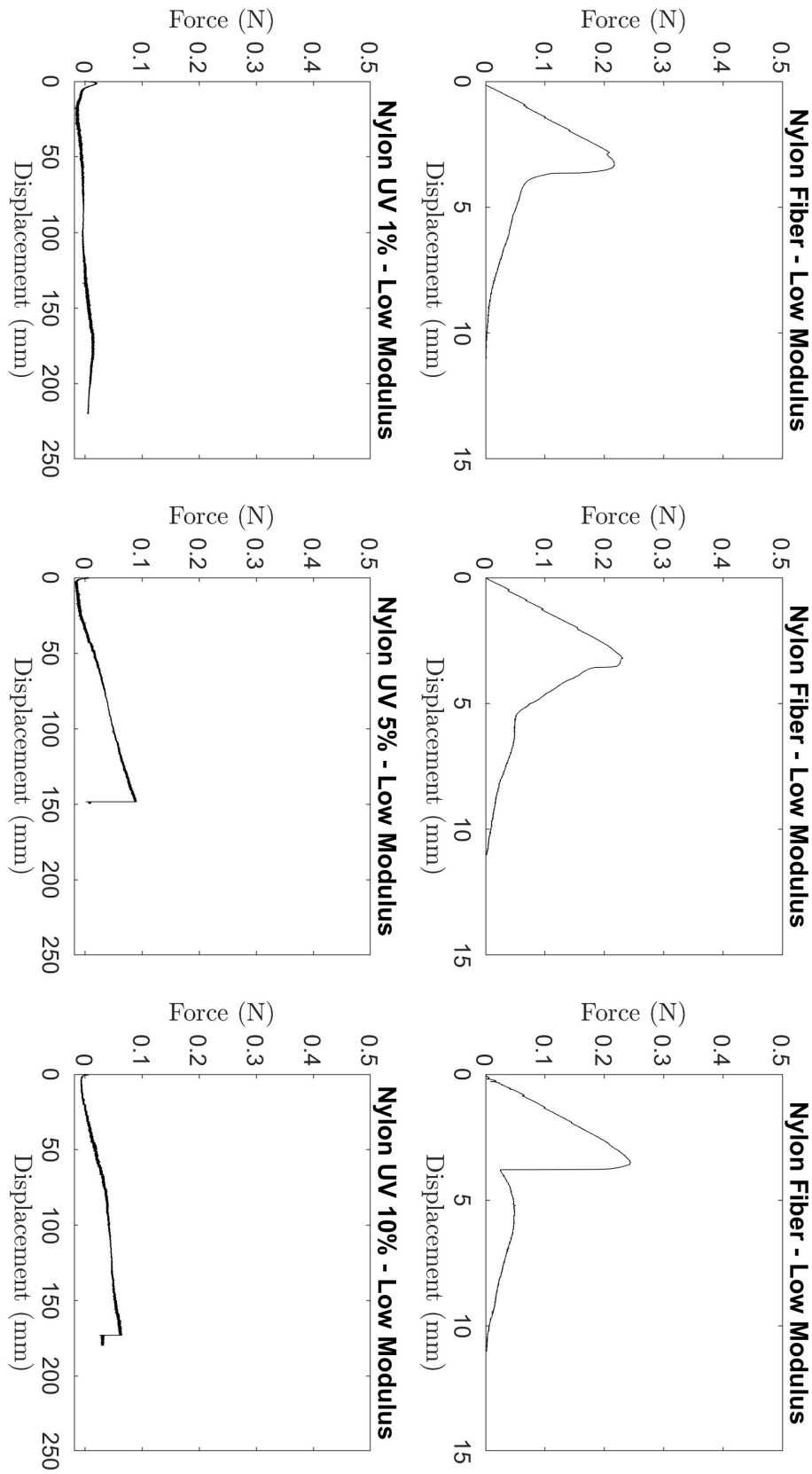


Figure A.7.: Detailed measurement results – nylon fiber & low material.

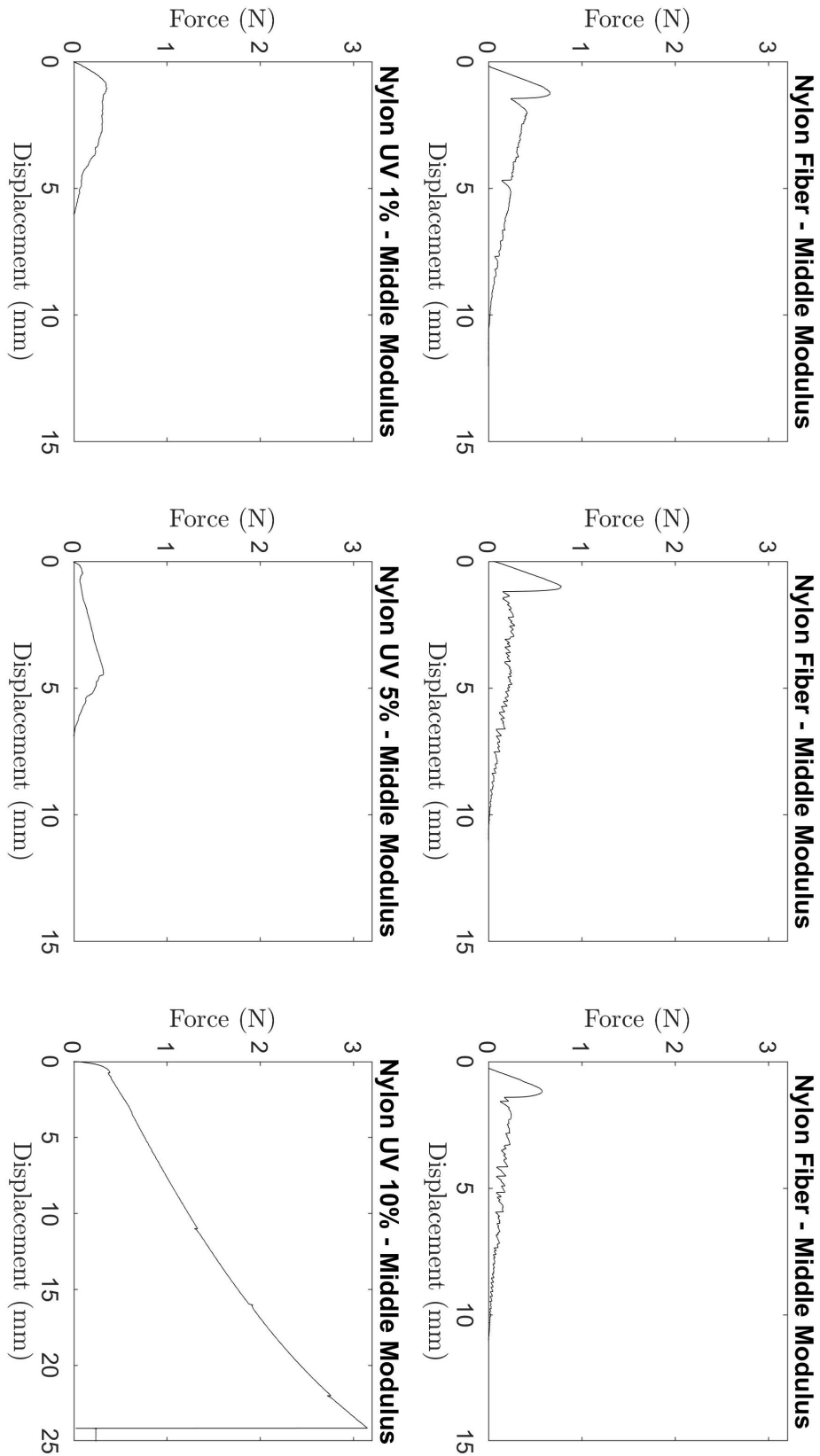


Figure A.8.: Detailed measurement results – nylon fiber & middle material.

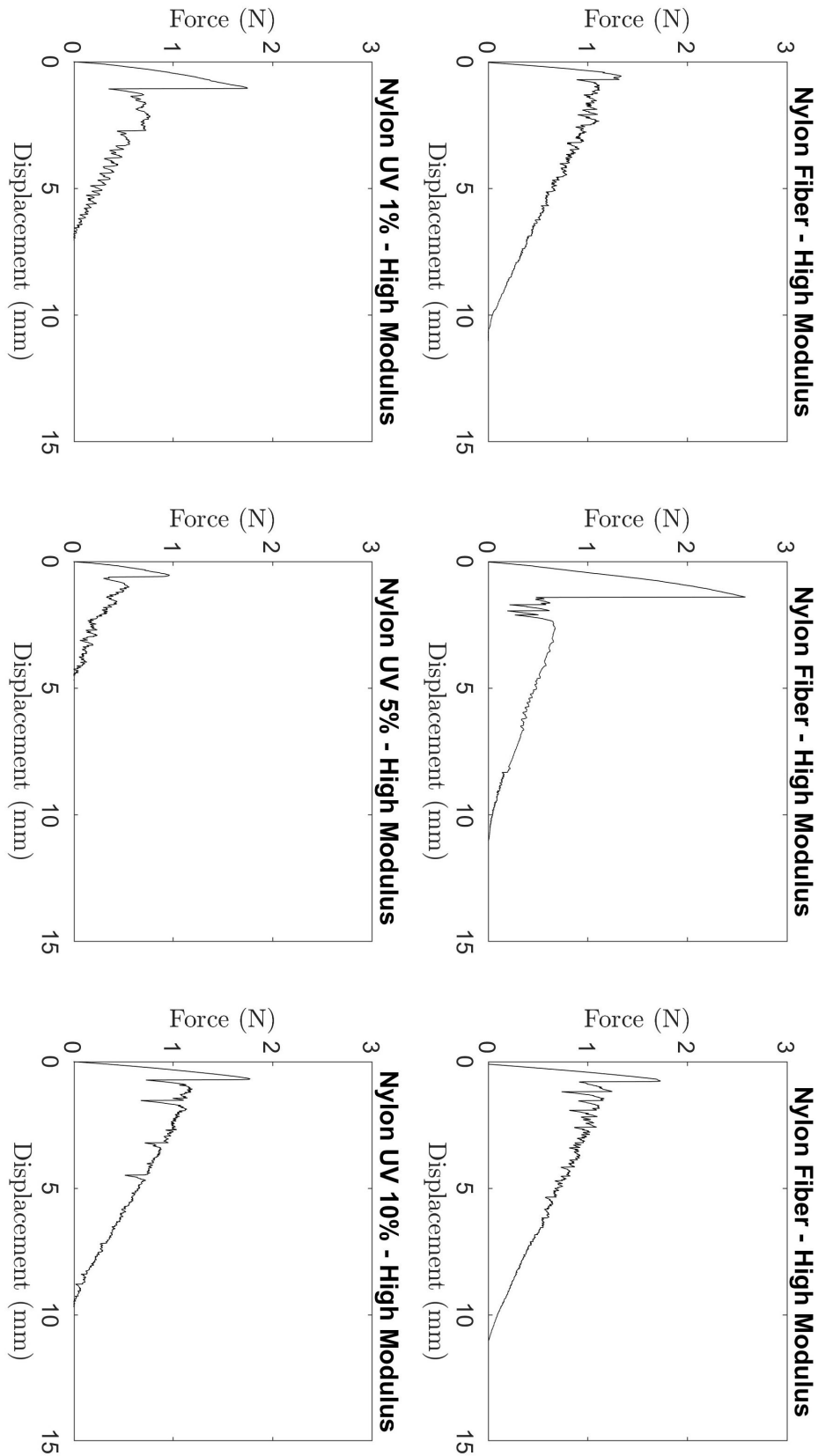


Figure A.9.: Detailed measurement results – nylon fiber & high material.

B. Source Code for Test Evaluation

B.1. Source Code for Evaluation of Test Data

```
1 % Read in the data to a table
  A1 = readtable('First_Test_8_5_2023_H_N.txt');
  A2 = readtable('Second_Test_8_5_2023_H_N.txt');
  A3 = readtable('Third_Test_8_5_2023_H_N.txt');
  A4 = readtable('UV_1_First_Test_9_5_2023_H_N.txt');
6 A5 = readtable('UV_5_First_Test_9_5_2023_H_N.txt');
  A6 = readtable('UV_10_First_Test_8_5_2023_H_N.txt');
  my_data1 = table2array(A1);
  my_data2 = table2array(A2);
  my_data3 = table2array(A3);
11 my_data4 = table2array(A4);
  my_data5 = table2array(A5);
  my_data6 = table2array(A6);

  % Create a figure with 6 subplots
16 figure
  subplot(2,3,1)
  all_disp1 = my_data1(:,3)-my_data1(1,3); % displacement values
  all_forces1 = my_data1(:,4)-my_data1(end,4); % force values
  plot(all_disp1, all_forces1, 'k')
21 xlabel('Displacement_(mm)', 'Interpreter', 'latex')
  ylabel('Force_(N)', 'Interpreter', 'latex')
  set(gca, 'FontSize', 15)
  axis([-0.15 -0.0 3])
  title('Nylon_Fiber_-_High_Modulus')
26
  subplot(2,3,2)
  all_disp2 = my_data2(:,3)-my_data2(1,3); % displacement values
  all_forces2 = my_data2(:,4)-my_data2(end,4); % force values
  plot(all_disp2, all_forces2, 'k')
31 xlabel('Displacement_(mm)', 'Interpreter', 'latex')
  ylabel('Force_(N)', 'Interpreter', 'latex')
  set(gca, 'FontSize', 15)
```

```

axis([-0.15 -0.0 3])
title('Nylon_Fiber_High_Modulus')
36
subplot(2,3,3)
all_disp3 = my_data3(:,3) - my_data3(1,3); % displacement values
all_forces3 = my_data3(:,4) - my_data3(end,4); % force values
plot(all_disp3, all_forces3, 'k')
41 xlabel('Displacement_(mm)', 'Interpreter', 'latex')
ylabel('Force_(N)', 'Interpreter', 'latex')
set(gca, 'FontSize', 15)
axis([-0.15 0 3])
title('Nylon_Fiber_High_Modulus')
46
subplot(2,3,4)
all_disp4 = my_data4(:,3) - my_data4(1,3); % displacement values
all_forces4 = my_data4(:,4) - my_data4(1,4); % force values
plot(all_disp4, all_forces4, 'k')
51 xlabel('Displacement_(mm)', 'Interpreter', 'latex')
ylabel('Force_(N)', 'Interpreter', 'latex')
set(gca, 'FontSize', 15)
axis([-0.15 0 3])
title('Nylon_UV_1%_High_Modulus')
56
subplot(2,3,5)
all_disp5 = my_data5(:,3) - my_data5(1,3); % displacement values
all_forces5 = my_data5(:,4) - my_data5(1,4); % force values
plot(all_disp5, all_forces5, 'k')
61 xlabel('Displacement_(mm)', 'Interpreter', 'latex')
ylabel('Force_(N)', 'Interpreter', 'latex')
set(gca, 'FontSize', 15)
axis([-0.15 0 3])
title('Nylon_UV_5%_High_Modulus')
66
subplot(2,3,6)
all_disp6 = my_data6(:,3) - my_data6(1,3); % displacement values
all_forces6 = my_data6(:,4) - my_data6(1,4); % force values
plot(all_disp6, all_forces6, 'k')
71 xlabel('Displacement_(mm)', 'Interpreter', 'latex')
ylabel('Force_(N)', 'Interpreter', 'latex')
set(gca, 'FontSize', 15)
axis([-0.15 0 3])
title('Nylon_UV_10%_High_Modulus')

```

B.2. Source Code for Creating a Heat-Map

```

% Define the data matrix (3x3) – replace with your own data
data = [3.541 3.715 1.259; 1.236 5.789 0.934; 1.066 0.739 0.953];

4 % Create a figure and set its size
figure('Position', [100, 100, 500, 400]);

% Define the colors for the heatmap
colormap([1 1 1; repmat(linspace(1, 0, 64)', 1, 3); 0 0 0]);

9
% Create the heatmap using the imagesc function
imagesc(data, [0, 6]);

% Adjust the color axis scaling
14 caxis([0, 6]);

% Set the aspect ratio to ensure square rectangles
pbaspect([3, 3, 1]);

19 % Set the tick labels and font sizes
yticks([1, 2, 3]);
yticklabels({'Nylon Fiber', 'Glass Fiber', 'Steel Fiber'});
xticks([1, 2, 3]);
xticklabels({'Low Material', 'Middle Material', 'High Material'});
24 set(gca, 'FontSize', 20);

% Display the color scale on the right side
colorbar('eastoutside');

29 % Add the text labels with opposite color to each rectangle
for i = 1:size(data, 1)
for j = 1:size(data, 2)
    value = data(i, j);
    if value < 3
34         text(j, i, num2str(value), 'Color', [0 0 0], 'FontSize', 20, ...
            'HorizontalAlignment', 'center', 'VerticalAlignment', 'middle');
    else
        text(j, i, num2str(value), 'Color', [1 1 1], 'FontSize', 20, ...
            'HorizontalAlignment', 'center', 'VerticalAlignment', 'middle');
39     end
end
end

```

```

end

%_Add_a_title_to_the_figure
44 title('Stiffness Ratio (UV off / UV on)', '_', 'FontSize', 20);

```

B.3. Source Code for Curve-Fitting

```

% create a new figure
figure;

4 % plot the data
h_data = plot(x - x(1), y - y(1), '-.', 'Color', [0.65 0.65 0.65],
'LineWidth', 1.5); % Dashed 0.65 grey line
xlabel('Displacement_(mm)', 'Interpreter', 'latex', 'FontSize', 16);
ylabel('Force_(N)', 'Interpreter', 'latex', 'FontSize', 16);
9 axis([0 8 0 1.4]);

% specify subset of data for linear fit
start_idx = 1; % index of first point to include in linear fit
end_idx = 180; % index of last point to include in linear fit
14

% perform linear fit using polyfit
p1 = polyfit(x(start_idx:end_idx) - x(1), y(start_idx:end_idx) - y(1), 1);

% plot linear fit along with data
19 hold on;
h_fit1 = plot(x(start_idx:end_idx) - x(1),
polyval(p1, x(start_idx:end_idx) - x(1)), 'k-', 'LineWidth', 2);
% Solid black line
hold off;

24

% display equation of linear fit
fprintf('y = %.4fx + %.4f\n', p1(1), p1(2));

% specify subset of data for linear fit
29 start_idx = 320; % index of first point to include in linear fit
end_idx = 1200; % index of last point to include in linear fit

% perform linear fit using polyfit
p2 = polyfit(x(start_idx:end_idx) - x(1), y(start_idx:end_idx)
34 - y(1), 1);

```

```
% plot linear fit along with data
hold on;
h_fit2 = plot(x(start_idx:end_idx) - x(1),
39 polyval(p2, x(start_idx:end_idx) - x(1)), 'k-', 'LineWidth', 2);
% Solid black line
hold off;

% display equation of linear fit
44 fprintf('y = %.4fx + %.4f\n', p2(1), p2(2));

% Adjust the font size of axis tick labels
set(gca, 'FontSize', 32);

49 % Add legend
legend([h_data, h_fit1, h_fit2], 'Experimental_Data',
'Curve_Fitting_1_-_Stiffness', 'Curve_Fitting_2_-_Friction', 'Location',
'northeast');

54 % Add title
title('Data_Evaluation', 'FontSize', 32, 'FontWeight', 'bold');
```